Research Square

Preprints are preliminary reports that have not undergone peer review.
They should not be considered conclusive, used to inform clinical practice,
or referenced by the media as validated information.

Fermionic perturbations and spinning particle dynamics in asymptotically safe charged black holes

Erdem Sucu

erdemsc07@gmail.com

Eastern Mediterranean University

izzet Sakallı

Eastern Mediterranean University

Research Article

Keywords: Black hole, Dirac Field, Thermodynamics, Quantum Corrections, Quasinormal Modes;Quality Factor, Tidal Force

Posted Date: March 12th, 2026

DOI: https://doi.org/10.21203/rs.3.rs-8836854/v1

License: This work is licensed under a Creative Commons Attribution 4.0 International License.
Read Full License

Additional Declarations: No competing interests reported.

Fermionic perturbations and spinning particle dynamics in asymptotically safe charged black holes

Erdem Sucu [1, *] and İzzet Sakallı [1, †]

[1] *Physics Department, Eastern Mediterranean University, Famagusta, 99628 North Cyprus, via Mersin 10, Türkiye*

(Dated: February 10, 2026)

We investigate a quantum-corrected charged black hole obtained by promoting the Newtonian coupling to a scale-dependent quantity, as motivated by renormalization group improvement in Quantum Einstein Gravity. This yields a modified Reissner-Nordstrm spacetime where quantum effects are encoded through radial running of the gravitational coupling, while the classical limit is recovered at large distances. Fermionic Hawking radiation is studied within a tunneling framework based on a Generalized Uncertainty Principle-deformed Dirac equation. The resulting Hawking temperature is reduced relative to the semiclassical case, reflecting minimal-length effects that propagate into the thermodynamic sector. We derive quantum-corrected internal energy, Helmholtz free energy, and pressure within the extended phase space formalism. Deviations from classical thermodynamics are most pronounced near the event horizon and become negligible in the weak-field regime. The dynamical response is examined through fermionic perturbations by constructing the effective potential and employing a semiclassical approximation to compute the quasinormal mode spectrum and quality factors. Results indicate that running gravitational coupling mainly affects damping properties with milder impact on oscillation frequencies. Tidal forces analyzed via the geodesic deviation equation reveal characteristic transition radii where the nature of tidal deformation changes due to quantum corrections. Finally, motion of spinning magnetized test particles is explored through an effective radial potential, showing that quantum corrections primarily modify dynamics in the strong-field region while leaving asymptotic behavior essentially classical. Our results demonstrate how scale-dependent gravity and minimal-length effects jointly modify both thermodynamic and dynamical properties of charged black holes.

Keywords: Black hole; Dirac Field ; Thermodynamics; Quantum Corrections; Quasinormal Modes;Quality Factor; Tidal Force.

I. INTRODUCTION

Black holes (BHs) represent the most extreme manifestations of gravitational physics, where spacetime curvature reaches its highest intensity and classical general relativity confronts its fundamental limitations. The Reissner-Nordström (RN) solution describes electrically charged BHs as one of the cornerstone exact solutions in Einstein's theory, yet it harbors curvature singularities at the origin where predictability breaks down [1–4]. This singular behavior has motivated decades of research into quantum gravitational corrections that might regularize the short-distance structure of BH spacetimes while preserving successful predictions at macroscopic scales [5–7].

Among theoretical frameworks for quantum gravity, the asymptotic safety program based on Quantum Einstein Gravity (QEG) has emerged as a promising approach [8–10]. The central hypothesis posits that gravity remains a consistent quantum field theory at arbitrarily high energies due to a non-Gaussian ultraviolet fixed point in the renormalization group (RG) flow [8, 11]. This scenario, first proposed by Weinberg [12], has received support from functional renormalization group calculations and offers an alternative to perturbatively non-renormalizable approaches [13–15]. The key ingredient is the running Newton constant (RNC), which replaces the fixed gravitational coupling G with a position-dependent function $G(r) = G_0 r^2/(r^2 + \alpha G_0)$, where G_0 is the asymptotic value and α parametrizes quantum corrections [16, 17]. This functional form exhibits antiscreening behavior where gravity weakens at short distances, potentially regularizing classical singularities [18].

Complementary to geometric modifications from running couplings, the Generalized Uncertainty Principle (GUP) [19–38] introduces a minimal measurable length scale by modifying the Heisenberg uncertainty relation. Emerging from string theory [23, 39, 40], loop quantum gravity [41–43], and gedanken experiments [44], the GUP relation $\Delta x \Delta p \geq \hbar(1 + \alpha_{\text{GUP}} \Delta p^2)/2$ establishes a minimum position uncertainty of order the Planck length. When implemented in relativistic wave equations, the GUP induces higher-derivative corrections that modify particle tunneling rates and Hawking radiation [45–50]. Combining RNCs (modifying background geometry) with GUP corrections (modifying quantum matter) provides a two-fold implementation of Planck-scale physics capturing complementary quantum gravitational effects.

Recent observational advances have opened unprecedented windows for testing BH physics in strong-field regimes. Gravitational wave detections by LIGO-Virgo-KAGRA provide precise measurements of ringdown frequencies encoding spacetime geometry [51–55], while Event Horizon Telescope imaging of BH shadows offers direct constraints on near-horizon structure [56–60]. These observations motivate detailed predictions for quantum-corrected BH solutions, particularly

* erdemsc07@gmail.com
† izzet.sakalli@emu.edu.tr

for observable quantities such as quasinormal mode (QNM) spectra that may deviate measurably from classical general relativity if quantum effects become significant at horizon scales.

QNMs represent characteristic oscillation and damping patterns of perturbations around BHs, providing unique fingerprints of spacetime geometry accessible through gravitational wave observations [61–72]. While scalar and gravitational perturbations have been extensively studied, fermionic perturbations remain comparatively less explored despite their fundamental role [63, 73–76]. Massless Dirac fields couple to curvature through spin connections, making them particularly sensitive to near-horizon modifications where quantum corrections are strongest. Fermionic QNM spectra exhibit distinct features compared to bosonic modes, with slower damping and quality factors increasing systematically with angular momentum [77–79].

Tidal forces experienced by extended objects provide another probe of curvature structure through the geodesic deviation equation [80–82]. In classical general relativity, tidal forces around charged BHs exhibit monotonic behavior throughout the exterior region. However, scale-dependent gravitational coupling can produce tidal inversions where stretching transitions to compression at specific radii determined by quantum parameters [83, 84], representing distinctive signatures with no classical counterpart. The motion of spinning test particles with magnetic dipole moments offers yet another window through the Mathisson-Papapetrou-Dixon (MPD) equations incorporating spin-curvature coupling and electromagnetic interactions [85–89]. In quantum-corrected geometries, the RNC modifies both gravitational potential depth and spin-curvature coupling terms, producing shifts in orbital structure that could affect accretion disk spectra.

In this work, we investigate a quantum-corrected charged BH (QCCBH) solution combining RNC modifications from asymptotic safety with GUP corrections to quantum matter dynamics. We examine geometric structure and horizon properties, establishing how $G(r)$ modifies extremality conditions. We analyze fermionic Hawking radiation through GUP-corrected Dirac tunneling, computing modified temperatures and examining implications for evaporation dynamics. The thermodynamic sector is explored through GUP-corrected entropy, internal energy, Helmholtz free energy, and thermodynamic pressure within the extended phase space framework. For dynamical properties, we derive the effective potential for Dirac perturbations and compute QNM frequencies using the Wentzel-Kramers-Brillouin (WKB) approximation, examining how quantum parameters influence oscillation frequencies, damping rates, and quality factors. We analyze tidal forces through geodesic deviation, identifying radii where tidal components change sign. Finally, we investigate spinning magnetized particle dynamics using the MPD formalism, deriving the effective potential incorporating spacetime curvature, spin-curvature coupling, magnetic interactions, and quantum corrections.

Our approach differs from previous studies by investigating combined influences of geometric modifications and GUP corrections on both thermodynamic and dynamical properties. We extend perturbative analysis to fermionic modes, which provide complementary information about near-horizon structure through distinctive damping properties. The tidal force investigation reveals qualitatively new inversion behaviors that could serve as signatures of quantum gravity in strong-field regimes.

The paper is organized as follows. Section II presents the metric structure, horizon locations, and extremality conditions. Section III develops GUP-corrected Dirac tunneling for fermionic Hawking radiation. Section IV analyzes thermodynamic properties within the extended phase space framework. Section V derives the effective potential for Dirac perturbations and computes QNM frequencies and quality factors. Section VI investigates tidal forces and derives transition radii. Section VII analyzes spinning magnetized particle dynamics. Section VIII summarizes findings and discusses observational prospects.

II. QCCBH GEOMETRY

The line element describing the QCCBH takes the standard static, spherically symmetric form

$$ds^2 = -f(r)\,dt^2 + \frac{dr^2}{f(r)} + r^2\left(d\theta^2 + \sin^2\theta\,d\phi^2\right), \quad (1)$$

where the metric function $f(r)$ incorporates the RNC and reads [17]

$$f(r) = 1 - \frac{2G(r)M}{r} + \frac{G(r)Q^2}{r^2}. \quad (2)$$

Here, M and Q represent the ADM mass and electric charge of the BH, respectively. The position-dependent gravitational coupling $G(r)$ encodes the leading quantum corrections arising from the asymptotic safety scenario.

Following the RNC prescription motivated by QEG [17], the running gravitational coupling is modeled as

$$G(r) = \frac{G_0 r^2}{r^2 + \omega G_0}, \quad (3)$$

where G_0 denotes the classical Newton constant measured at asymptotically large distances, and $\omega > 0$ is the quantum correction parameter controlling the magnitude of deviations from classical gravity. The functional form in Eq. (3) exhibits two important limiting behaviors: (i) $G(r) \to G_0$ as $r \to \infty$, recovering Newtonian gravity at large scales where quantum effects become negligible; and (ii) $G(r) \to 0$ as $r \to 0$, which progressively weakens gravitational attraction and softens the central singularity. This antiscreening behavior—gravity becoming weaker at shorter distances—is a hallmark signature of asymptotically safe gravity that distinguishes it from other quantum gravity approaches [17].

Substituting Eq. (3) into Eq. (2), the metric function can be written explicitly as

$$f(r) = 1 - \frac{2G_0 M r}{r^2 + \omega G_0} + \frac{G_0 Q^2}{r^2 + \omega G_0}. \quad (4)$$

The horizon structure is determined by the roots of $f(r) = 0$. After algebraic manipulation, the outer (r_+) and inner (r_-) horizon radii are found to be

$$r_\pm = G_0 M \pm \sqrt{(G_0 M)^2 - G_0\omega - G_0 Q^2}. \tag{5}$$

The existence of real-valued horizons requires the discriminant to be non-negative, yielding the condition

$$(G_0 M)^2 \geq G_0 \left(\omega + Q^2\right). \tag{6}$$

When the equality holds in Eq. (6), the two horizons coalesce into a single degenerate horizon at $r_{\text{ext}} = G_0 M$, corresponding to an extremal BH configuration with vanishing surface gravity. For parameters violating Eq. (6), no horizon exists and the spacetime contains a naked singularity.

The critical charge Q_{crit} separating BH solutions from naked singularities is obtained from the extremality condition:

$$Q_{\text{crit}} = \sqrt{G_0 M^2 - \omega}. \tag{7}$$

A notable consequence of Eq. (7) is that the quantum parameter ω reduces the critical charge compared to the classical RN case, where $Q_{\text{crit}}^{\text{RN}} = \sqrt{G_0} M$. This indicates that quantum corrections effectively shrink the parameter space admitting regular BH solutions, making naked singularity formation more likely for a given mass. The implications of this feature for cosmic censorship and the endpoint of Hawking evaporation deserve further investigation.

Table I summarizes the horizon structure for representative parameter choices with $G_0 = 1$ and $M = 1$, illustrating the transition from non-extremal BHs through extremal configurations to naked singularities as the charge-to-mass ratio increases. The table clearly shows that increasing ω at fixed Q pushes the horizons closer together (reducing $\Delta r = r_+ - r_-$), while increasing Q at fixed ω has a similar effect until extremality is reached.

Figure 1 displays the radial profile of the metric function $f(r)$ for various combinations of Q and ω, clearly distinguishing non-extremal BHs (two distinct zeros), extremal BHs (single degenerate zero), and naked singularities (no zeros). The solid curves correspond to the classical RN limit ($\omega = 0$), while dashed and dash-dotted curves represent quantum-corrected cases with $\omega = 0.1$ and $\omega = 0.3$, respectively. Different colors indicate the charge regime: navy blue for non-extremal BHs with $Q = 0.3$, orange for near-extremal configurations with $Q = 0.6$–0.7, green for extremal BHs at $Q = Q_{\text{crit}}(\omega)$, and crimson for naked singularities (NS) with $Q > Q_{\text{crit}}$.

As the quantum parameter ω increases, the potential barrier near the origin becomes more pronounced due to the weakening of gravity at short distances. This behavior reflects the antiscreening nature of the RNC, which effectively repels the inner horizon outward while pushing the outer horizon inward, ultimately merging them at the extremal configuration. For $Q > Q_{\text{crit}}$, the metric function remains positive for all $r > 0$, indicating the absence of horizons and the exposure of the central region to external observers.

In the limit $\omega \to 0$, the classical RN geometry is recovered with horizon radii $r_\pm^{\text{RN}} = G_0 M \pm \sqrt{(G_0 M)^2 - G_0 Q^2}$.

TABLE I. Horizon radii $r_\pm$ for the QCCBH with $G_0 = 1$ and $M = 1$. The critical charge is $Q_{\text{crit}} = \sqrt{G_0 M^2 - \omega}$. Entries "—" denote naked singularities (NS).

ω	Q	r_+	r_-	Configuration
		Classical RN limit		
0.00	0.000	2.000	0.000	Schwarzschild
0.00	0.300	1.954	0.046	Non-extremal
0.00	0.500	1.866	0.134	Non-extremal
0.00	0.700	1.714	0.286	Non-extremal
0.00	1.000	1.000	1.000	Extremal
0.00	1.100	—	—	NS
		Quantum-corrected ($\omega = 0.1$)		
0.10	0.000	1.949	0.051	Schwarzschild
0.10	0.300	1.900	0.100	Non-extremal
0.10	0.500	1.806	0.194	Non-extremal
0.10	0.700	1.640	0.360	Non-extremal
0.10	0.949	1.000	1.000	Extremal
0.10	1.100	—	—	NS
		Quantum-corrected ($\omega = 0.3$)		
0.30	0.000	1.837	0.163	Schwarzschild
0.30	0.300	1.781	0.219	Non-extremal
0.30	0.500	1.671	0.329	Non-extremal
0.30	0.700	1.458	0.542	Non-extremal
0.30	0.837	1.000	1.000	Extremal
0.30	1.100	—	—	NS

Conversely, for fixed Q, increasing ω progressively reduces the horizon separation $\Delta r = r_+ - r_-$ until extremality is reached at $\omega_{\text{ext}} = G_0 M^2 - Q^2$. Beyond this point, the spacetime transitions to a naked singularity configuration. This quantum-induced shrinking of the BH parameter space has potential implications for cosmic censorship and merits further study in the context of gravitational collapse.

The surface gravity at the outer horizon, which determines the Hawking temperature in the semiclassical approximation, is given by

$$\kappa = \frac{1}{2}\left.\frac{df}{dr}\right|_{r=r_+} = \frac{r_+ - r_-}{2r_+^2 + 2\omega G_0}. \tag{8}$$

For extremal BHs where $r_+ = r_-$, we have $\kappa = 0$, implying a vanishing Hawking temperature and a thermodynamically stable configuration. The presence of ω in the denominator of Eq. (8) indicates that quantum corrections further suppress the surface gravity even for non-extremal configurations, leading to cooler BHs compared to their classical counterparts. This feature will be central to the GUP-corrected thermodynamic analysis presented in Sec. III.

III. GUP-CORRECTED DIRAC TUNNELING AND HAWKING RADIATION

The semiclassical treatment of BH thermodynamics, pioneered by Bekenstein and Hawking [90, 91], predicts that BHs radiate thermal particles with a characteristic temperature inversely proportional to their mass. This remarkable result connects gravity, quantum mechanics, and thermodynamics in a profound manner, yet it relies on quantum field

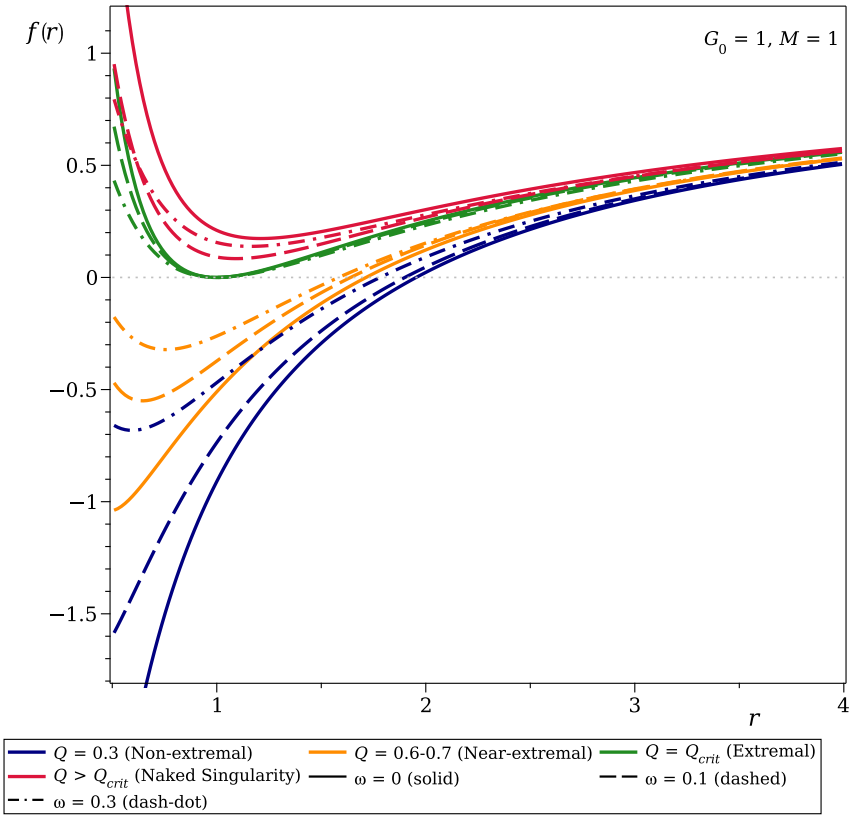


FIG. 1. Metric function $f(r)$ for the QCCBH with $G_0 = 1$ and $M = 1$. Line styles distinguish values of the quantum parameter: solid ($\omega = 0$, classical RN limit), dashed ($\omega = 0.1$), and dash-dotted ($\omega = 0.3$). Colors indicate charge regimes: navy blue ($Q = 0.3$, non-extremal), orange ($Q = 0.6$–0.7, near-extremal), green ($Q = Q_{\rm crit}$, extremal), and crimson ($Q > Q_{\rm crit}$, naked singularity). The horizontal dotted line marks $f(r) = 0$.

theory in curved spacetime where the background geometry is treated classically [92–94]. At energy scales approaching the Planck regime, both the spacetime structure and the quantum mechanical description of matter are expected to receive modifications from a yet-unknown theory of quantum gravity [95, 96].

One of the most widely studied phenomenological approaches to incorporate Planck-scale effects into quantum mechanics is the GUP [28, 97–101]. The GUP emerges from various candidate theories of quantum gravity, including string theory, loop quantum gravity, and gedanken experiments involving gravitational effects on position measurements. The common feature of these approaches is the prediction of a minimal measurable length, typically of order the Planck length $\ell_P = \sqrt{\hbar G_0/c^3} \approx 1.6 \times 10^{-35}$ m, below which the classical notion of spacetime loses operational meaning [40].

The GUP modifies the canonical Heisenberg uncertainty relation according to [102]

$$\Delta x\, \Delta p \geq \frac{\hbar}{2}\left(1 + \alpha\, \Delta p^2\right), \tag{9}$$

where $\alpha = \alpha_0/M_P^2 c^2$ is the GUP deformation parameter, with α_0 a dimensionless constant of order unity and M_P the Planck mass. The inequality in Eq. (9) implies that $\Delta x \geq \hbar\sqrt{\alpha}$, establishing a minimum uncertainty in position measurements. This modification leads to a deformed algebra between position and momentum operators [103]:

$$[x, p] = i\hbar\left(1 + \alpha p^2\right), \tag{10}$$

which in turn induces higher-derivative corrections to relativistic wave equations [104].

The combination of GUP-modified quantum mechanics with quantum-corrected BH geometries provides a two-fold implementation of Planck-scale physics: the RNC modifies the background spacetime as discussed in Sec. II, while the GUP alters the dynamics of quantum fields propagating on this background. This dual approach captures complementary aspects of quantum gravity effects and leads to distinctive predictions for Hawking radiation that differ from either modification alone [46, 105].

Within the GUP framework, the dynamics of a massive charged fermion in curved spacetime is governed by a deformed Dirac equation. Following the approach developed in Refs. [106–108], both the kinetic and mass terms receive leading-order $\mathcal{O}(\alpha)$ corrections. In a general static background, the GUP-modified Dirac equation takes the

schematic form

$$\left[i\gamma^{\mu}(x)\nabla_{\mu}-\frac{m_0}{\hbar}\right]\tilde{\Psi}+\alpha\,\mathcal{D}_{\rm GUP}\tilde{\Psi}=0, \tag{11}$$

where $\gamma^{\mu}(x)$ denote the curved-space gamma matrices satisfying the Clifford algebra $\{\gamma^{\mu},\gamma^{\nu}\}=2g^{\mu\nu}$, ∇_{μ} is the spinor covariant derivative including the spin connection, and $\mathcal{D}_{\rm GUP}$ encodes higher-derivative operators arising from the GUP. In the limit $\alpha\to 0$, the standard Dirac equation in curved spacetime is recovered [109–111].

To investigate fermionic Hawking radiation from the QCCBH, we employ the semiclassical tunneling method originally developed by Parikh and Wilczek [112] for scalar particles and subsequently extended to fermions by Kerner and Mann [113]. This approach treats Hawking emission as a quantum tunneling process through the classically forbidden region at the horizon, with the tunneling probability determined by the imaginary part of the particle's classical action [114]. The method has been successfully applied to various BH spacetimes and field types, providing results consistent with the original Hawking calculation while offering additional physical transparency [115].

We adopt a WKB ansatz for the outgoing spin-up solution of the form

$$\tilde{\Psi}(t,r,\theta,\varphi)=\exp\!\left(\frac{i}{\hbar}S(t,r,\theta,\varphi)\right)\begin{pmatrix}A\\0\\B\\0\end{pmatrix}, \tag{12}$$

where S denotes the classical action and A, B are spinor amplitudes to be determined. Substituting this ansatz into the GUP-modified Dirac equation (11) and retaining only leading-order terms in $\hbar$ yields a set of algebraic equations for the spinor amplitudes. The consistency condition for non-trivial solutions leads to a deformed Hamilton–Jacobi equation governing the particle trajectory [113, 116].

Assuming separability of the action in the form

$$S=-Et+j\varphi+R(r)+W(\theta)+C, \tag{13}$$

where E is the particle energy, j the azimuthal quantum number, $R(r)$ the radial action, $W(\theta)$ the angular part, and C an integration constant, and eliminating the angular sector through standard techniques, one obtains a GUP-corrected radial Hamilton–Jacobi equation. For the QCCBH metric characterized by the lapse function $f(r)$ given in Eq. (4), the radial equation reads

$$\frac{1}{f(r)}(E-qA_0)^2-f(r)\left(\frac{dR}{dr}\right)^2-m_0^2+\alpha\,\mathcal{F}(E,m_0,A_0,f)=0, \tag{14}$$

where q is the fermion charge, A_0 the electromagnetic potential, and $\mathcal{F}$ collects all $\mathcal{O}(\alpha)$ contributions from the GUP. The first three terms reproduce the standard Hamilton–Jacobi equation for a Dirac particle in a static charged BH background, while the additional term encodes GUP-induced quantum corrections.

Solving Eq. (14) for the radial action yields the outgoing $(+)$ and ingoing $(-)$ solutions

$$R_{\pm}(r)=\pm\int\frac{\sqrt{(E-qA_0)^2-f(r)m_0^2}}{f(r)}\left[1+\alpha\,\mathcal{C}(r)\right]dr, \tag{15}$$

where $\mathcal{C}(r)$ represents the explicit GUP correction factor that depends on the metric function and particle parameters. Near the event horizon $r=r_+$, the metric function exhibits a linear behavior

$$f(r)\simeq f'(r_h)(r-r_h)+\mathcal{O}\left((r-r_+)^2\right), \tag{16}$$

leading to a simple pole in the integrand of Eq. (15). This pole structure is responsible for the imaginary contribution to the action that determines the tunneling probability.

Evaluating the integral by deforming the contour in the complex r-plane around the pole at $r=r_h$ yields the imaginary part of the radial action [117]:

$$\mathrm{Im}\,R_{\pm}=\pm\frac{\pi E}{f'(r_h)}\left(1+\alpha\,\Xi\right), \tag{17}$$

where the dimensionless quantity Ξ encapsulates the leading GUP contribution and depends on the particle mass, energy, and the surface gravity at the horizon. For neutral emission $(q=0)$, Ξ takes the explicit form

$$\Xi=\frac{3m_0^2f'(r_h)}{2E}, \tag{18}$$

while for charged fermions additional terms involving the electromagnetic potential $A_0(r_h)$ appear.

The tunneling probability is determined by the difference between the imaginary parts of the outgoing and ingoing actions:

$$\begin{aligned}\Gamma&=\frac{P_{\rm emission}}{P_{\rm absorption}}=\exp(-2\,\mathrm{Im}\,R_{+}+2\,\mathrm{Im}\,R_{-})\\&=\exp\!\left(-\frac{4\pi E}{f'(r_+)}\left[1+\alpha\,\Xi\right]\right).\end{aligned} \tag{19}$$

Comparing this expression with the Boltzmann factor $\Gamma=\exp(-E/T)$ for thermal emission, the GUP-corrected Hawking temperature is identified as

$$T_{\rm GUP}=\frac{f'(r_+)}{4\pi\left(1+\alpha\,\Xi\right)}=\frac{T_H^D}{1+\alpha\,\Xi}, \tag{20}$$

where $T_H^D=f'(r_h)/(4\pi)$ denotes the standard Dirac Hawking temperature in the absence of GUP corrections.

For the QCCBH metric, the derivative of the metric function at the outer horizon can be computed from Eq. (4):

$$f'(r_+)=\frac{2G_0M\left(r_h^2-\omega G_0\right)-2G_0Q^2r_h}{\left(r_h^2+\omega G_0\right)^2}. \tag{21}$$

Substituting the horizon radius from Eq. (5) and simplifying, the surface gravity can be related to the horizon separation as shown in Eq. (8). The GUP correction factor $(1+\alpha\Xi)^{-1}$

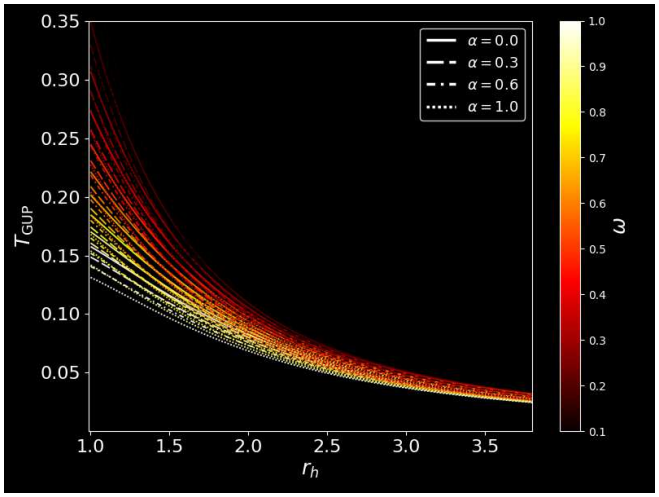


FIG. 2. GUP-corrected Hawking temperature $T_{\rm GUP}$ as a function of the horizon radius r_h for different values of the GUP parameter: $\alpha = 0.0$ (solid), 0.3 (dashed), 0.6 (dash-dotted), and 1.0 (dotted). The parameters are $G_0 = 1$, $M = 1$, $Q = 0.2$, and $\Xi = 0.2$. The color gradient indicates the variation of α.

then provides an additional suppression of the Hawking temperature beyond the quantum-geometric effects encoded in the RNC.

Figure 2 displays the behavior of the GUP-corrected Hawking temperature $T_{\rm GUP}$ as a function of the horizon radius r_h for different values of the GUP parameter α. The solid, dashed, dash-dotted, and dotted curves correspond to $\alpha = 0.0$, 0.3, 0.6, and 1.0, respectively, with the remaining parameters fixed at $G_0 = 1$, $M = 1$, $Q = 0.2$, and $\Xi = 0.2$. The figure reveals several important features of GUP-modified Hawking radiation from the QCCBH.

The most prominent feature of Fig. 2 is the monotonic reduction of the Hawking temperature with increasing α. For all values of the GUP parameter, $T_{\rm GUP}$ attains a maximum at intermediate horizon radii before decreasing toward zero at both small and large r_h. The peak temperature is progressively lowered as α increases, while the overall shape of the curve remains qualitatively unchanged. This behavior confirms that GUP corrections do not introduce new extrema in the temperature profile but rather rescale the temperature by the factor $(1 + \alpha\Xi)^{-1}$ throughout the parameter space.

The physical interpretation of this suppression is that quantum-gravitational effects associated with the minimal length scale reduce the efficiency of fermionic Hawking emission. Near the event horizon, where the local temperature is highest, the GUP correction becomes most relevant. Since $\Xi > 0$ for physically admissible particle parameters [cf. Eq. (18)], the temperature decrease is unavoidable and grows monotonically with α. This implies a slower evaporation rate compared to the standard semiclassical scenario, consistent with the general expectation that Planck-scale physics should regulate the divergent behavior of Hawking radiation for small BHs.

At larger horizon radii, $T_{\rm GUP}$ rapidly decreases and asymptotically approaches zero, indicating that quantum corrections do not alter the expected far-field behavior. The influence of the GUP is predominantly a near-horizon phenomenon, consistent with its origin in Planck-scale physics where spacetime curvature and quantum effects are strongest. This localization of GUP effects near the horizon supports the physical picture that quantum gravity modifications become significant only in regions of extreme gravitational fields [46, 47, 118].

The suppression of Hawking temperature has important implications for the late-stage evolution of BHs. In the standard semiclassical picture, the temperature diverges as the BH mass approaches zero, leading to an explosive endpoint of evaporation [91, 93]. The GUP correction mitigates this runaway behavior by reducing the temperature, potentially stabilizing the BH against complete evaporation and favoring the formation of long-lived remnants [119, 120]. Such remnants, with masses of order the Planck mass, have been proposed as candidates for dark matter and may carry information about the initial BH state, offering a possible resolution to the information paradox [121].

IV. GUP-CORRECTED THERMODYNAMIC QUANTITIES

The thermodynamics of BHs has been a central topic in gravitational physics since the seminal works of Bekenstein and Hawking established the proportionality between entropy and horizon area [90]. The extension of classical thermodynamic concepts to BH systems has led to remarkable parallels with ordinary thermodynamics, including phase transitions, critical phenomena, and equations of state [122]. In recent years, the extended phase space (EPS) formalism has gained considerable attention, wherein the cosmological constant is promoted to a thermodynamic variable interpreted as pressure, with the conjugate quantity being a thermodynamic volume [123, 124]. This framework has revealed rich phase structures in various BH solutions, including van der Waals-like behavior and reentrant phase transitions [125, 126].

The incorporation of quantum gravity effects into BH thermodynamics introduces modifications that probe the foundations of the Bekenstein-Hawking paradigm [90, 91]. As discussed in Sec. III, the GUP implies a minimal length scale that alters the near-horizon quantum field dynamics and consequently modifies the Hawking temperature. These modifications propagate through all thermodynamic relations, leading to GUP-corrected expressions for entropy, internal energy, free energy, and other state functions. The combination of GUP effects with the RNC prescription for the QCCBH provides a two-fold quantum gravity modification of the thermodynamic properties.

In this section, we analyze the thermodynamic properties of the QCCBH by incorporating the leading-order GUP corrections. The quantum-corrected Hawking temperature $T_{\rm GUP}$ given in Eq. (20) modifies the standard thermodynamic relations through the deformation factor $(1 + \alpha\Xi)^{-1}$, where α denotes the GUP parameter and Ξ encodes the particle-dependent correction defined in Eq. (18). This suppression factor appears universally in all thermodynamic

quantities derived from the modified temperature, leading to a consistent reduction of thermal properties compared to the semiclassical limit.

A. GUP-corrected entropy

The Bekenstein-Hawking entropy for a classical BH is given by the area law $S_{\rm BH} = A/(4G_0\hbar)$, where $A = 4\pi r_+^2$ is the horizon area [127]. Quantum gravity corrections to this formula have been extensively studied, with logarithmic corrections arising from various approaches including loop quantum gravity, string theory, and conformal field theory methods [43, 128]. The GUP introduces additional modifications that reflect the minimal length scale in the entropy-area relation [23, 129].

For the QCCBH with RNC, the corrected entropy incorporating GUP effects can be written as

$$S_{\rm GUP} = \frac{\pi r_+^2}{G_0\,(1+\alpha\Xi)}\left(1+\frac{\omega G_0}{r_+^2}\right)^{-1}, \tag{22}$$

where the factor $(1+\alpha\Xi)^{-1}$ arises from the GUP modification and the second factor accounts for the running of the gravitational coupling. In the limits $\alpha \to 0$ and $\omega \to 0$, the standard Bekenstein-Hawking result is recovered. The presence of both correction factors indicates that quantum effects from the GUP and the RNC act in the same direction, both reducing the entropy relative to the classical value.

B. Corrected internal energy

The internal energy of a thermodynamic system represents the total energy stored in its microscopic degrees of freedom. For BHs, the internal energy is related to the ADM mass through thermodynamic identities, with quantum corrections modifying this relationship [124, 130]. The GUP-corrected internal energy is obtained by integrating the Hawking temperature with respect to the corrected entropy:

$$E_{\rm GUP} = \int T_{\rm GUP}\, dS_{\rm GUP}, \tag{23}$$

which yields the explicit expression

$$\begin{aligned} E_{\rm GUP} = {} & \frac{G_0^2 M\omega}{(1+\alpha\Xi)\left(\omega G_0 + r_+^2\right)} + \frac{G_0 Q^2 r_+}{2\,(1+\alpha\Xi)\left(\omega G_0 + r_+^2\right)} \\ & + \frac{G_0 M}{2\,(1+\alpha\Xi)}\ln\!\left(\omega G_0 + r_+^2\right) \\ & - \frac{G_0 Q^2}{2\,(1+\alpha\Xi)\sqrt{\omega G_0}}\arctan\!\left(\frac{r_+}{\sqrt{\omega G_0}}\right). \end{aligned} \tag{24}$$

The structure of Eq. (24) reveals several notable features. The GUP correction factor $(1+\alpha\Xi)^{-1}$ appears as an overall multiplicative suppression, reducing the internal energy relative to its semiclassical counterpart throughout the parameter space. The logarithmic term originates from the integration of the temperature over the entropy, while the arctangent contribution arises from the charge-dependent sector and reflects the nontrivial coupling between the electric field and the RNC.

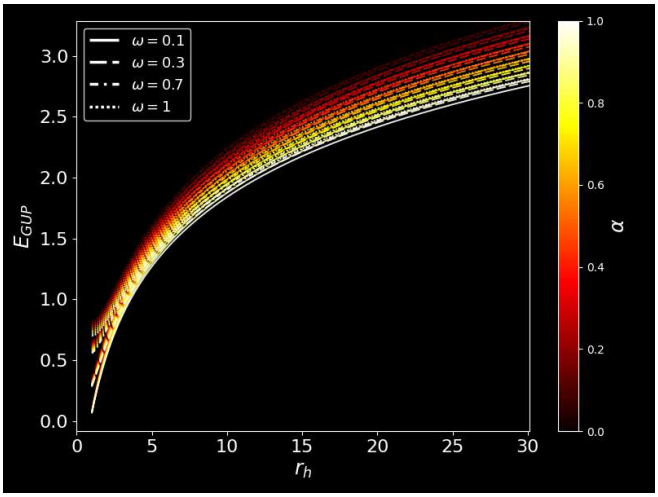


FIG. 3. GUP-corrected internal energy $E_{\rm GUP}$ as a function of the horizon radius r_h for different values of the quantum parameter: $\omega = 0.1$ (solid), 0.3 (dashed), 0.7 (dash-dotted), and 1.0 (dotted). The GUP parameter α varies as indicated by the color gradient. Other parameters: $G_0 = 1$, $M = 1$, $Q = 0.2$, $\Xi = 0.2$.

Figure 3 displays the radial dependence of the GUP-corrected internal energy $E_{\rm GUP}$ as a function of the horizon radius r_h for different values of the quantum parameter ω. The solid, dashed, dash-dotted, and dotted curves correspond to $\omega = 0.1$, 0.3, 0.7, and 1.0, respectively, while the GUP parameter α is kept fixed. The remaining parameters are chosen as $G_0 = 1$, $M = 1$, $Q = 0.2$, and $\Xi = 0.2$. The color gradient indicates the variation of α across the surface.

The figure demonstrates that $E_{\rm GUP}$ is a monotonically increasing function of the horizon radius, consistent with the thermodynamic expectation that larger BHs possess greater internal energy. The monotonic behavior also indicates thermodynamic stability with respect to variations in the horizon size, as the specific heat $C = dE/dT$ remains well-defined throughout the parameter range considered.

A comparison among the curves reveals that increasing ω leads to a suppression of the internal energy at fixed horizon radius. This effect is most pronounced for small values of r_h, where the RNC deviates most strongly from the classical Newton constant. The physical origin of this suppression lies in the weakening of the effective gravitational interaction through the running coupling $G(r) = G_0 r^2/(r^2 + \omega G_0)$, which reduces the gravitational binding energy in the near-horizon region. For large horizon radii, all curves converge toward a common asymptotic behavior, reflecting the recovery of classical thermodynamics in the weak-field regime where $G(r) \approx G_0$.

C. Helmholtz free energy

The Helmholtz free energy $F = E - TS$ measures the maximum work extractable from a thermodynamic system at constant temperature and volume [131]. For BH thermodynamics, the free energy plays a central role in determining phase stability and transition temperatures, with negative values indicating thermodynamically preferred configurations [132]. The GUP-corrected Helmholtz free energy is obtained from the standard thermodynamic relation

$$F_{\rm GUP} = E_{\rm GUP} - T_{\rm GUP} S_{\rm GUP} = -\int S_{\rm GUP}\, dT_{\rm GUP}, \quad (25)$$

leading to the explicit expression

$$\begin{aligned} F_{\rm GUP} = {} & \frac{3G_0^3 M\omega^2}{2\left(1+\alpha\Xi\right)\left(\omega G_0 + r_+^2\right)^2} + \frac{5G_0^2 M\omega r_+^2}{2\left(1+\alpha\Xi\right)\left(\omega G_0 + r_+^2\right)^2} \\ & + \frac{G_0^2 Q^2 \omega r_+}{2\left(1+\alpha\Xi\right)\left(\omega G_0 + r_+^2\right)^2} + \frac{G_0 Q^2 r_+^3}{\left(1+\alpha\Xi\right)\left(\omega G_0 + r_+^2\right)^2} \\ & + \frac{G_0 M}{2\left(1+\alpha\Xi\right)} \ln\!\left(\omega G_0 + r_+^2\right) \\ & - \frac{G_0 Q^2}{2\left(1+\alpha\Xi\right)\sqrt{\omega G_0}} \arctan\!\left(\frac{r_+}{\sqrt{\omega G_0}}\right). \end{aligned} \quad (26)$$

The Helmholtz free energy in Eq. (26) exhibits a more complex structure than the internal energy, with additional polynomial terms in the numerator arising from the entropy contribution. The logarithmic and arctangent terms persist from the internal energy expression, while the GUP correction factor $(1+\alpha\Xi)^{-1}$ again appears as a global suppression. The algebraic terms with higher powers of ω in the numerator indicate that the RNC modifications become increasingly important for the free energy compared to the internal energy.

Figure 4 illustrates the behavior of the GUP-corrected Helmholtz free energy $F_{\rm GUP}$ as a function of the horizon radius r_h for different values of the quantum parameter ω. The curve styles and parameter choices follow the same convention as in Fig. 3.

As shown in Fig. 4, the free energy $F_{\rm GUP}$ exhibits monotonically increasing behavior with the horizon radius, reflecting the balance between internal energy and the entropy-temperature product in the quantum-corrected thermodynamic framework. The positive values of $F_{\rm GUP}$ throughout the displayed range indicate that the QCCBH configurations considered here are thermodynamically less favorable compared to empty space at the same temperature, consistent with the expected behavior for small charged BHs [133].

Increasing ω shifts the free energy toward lower values at fixed horizon radius, following the same trend observed for the internal energy. This reduction indicates that quantum corrections encoded in the RNC diminish the thermodynamic potential available for work extraction from the BH system. The separation between curves is most significant in the small-r_h regime, where both the GUP and RNC effects are strongest, while convergence at large radii signals the restoration of classical behavior.

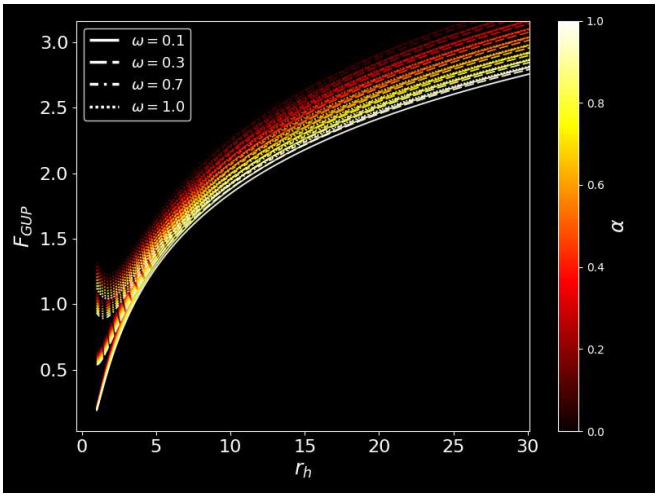


FIG. 4. GUP-corrected Helmholtz free energy $F_{\rm GUP}$ as a function of the horizon radius r_h for different values of the quantum parameter: $\omega = 0.1$ (solid), 0.3 (dashed), 0.7 (dash-dotted), and 1.0 (dotted). The GUP parameter α varies as indicated by the color gradient. Other parameters: $G_0 = 1$, $M = 1$, $Q = 0.2$, $\Xi = 0.2$.

From a thermodynamic stability perspective, the monotonic increase of $F_{\rm GUP}$ with r_h implies that smaller BHs are thermodynamically preferred at fixed temperature, a feature that would drive evaporation toward smaller masses in the absence of other stabilizing mechanisms. However, as discussed in Sec. III, the GUP-induced suppression of the Hawking temperature counteracts this tendency and may lead to the formation of stable remnants.

D. Pressure and EPS thermodynamics

The EPS formalism extends BH thermodynamics by treating the cosmological constant Λ as a dynamical variable identified with thermodynamic pressure through $P = -\Lambda/(8\pi G_0)$ [124, 134]. The conjugate thermodynamic volume V is then determined by the first law of BH thermodynamics, and the resulting framework exhibits rich phase behavior analogous to ordinary fluid systems [124, 135]. For asymptotically flat BHs without a cosmological constant, the EPS formalism can still be applied by defining an effective pressure through the variation of the free energy with respect to the thermodynamic volume [136, 137].

Within this framework, the GUP-corrected thermodynamic pressure is defined as

$$P_{\rm GUP} = -\frac{\partial F_{\rm GUP}}{\partial V}, \quad (27)$$

where the thermodynamic volume is identified with the naive geometric volume $V = 4\pi r_+^3/3$. Differentiating Eq. (26) with respect to V and using $\partial r_+/\partial V = (4\pi r_+^2)^{-1}$ yields the explicit expression

$$P_{\rm GUP} = -\frac{G_0\left(M r_+^3 - 3M\omega r_+ G_0 - \frac{3}{2}Q^2 r_+^2 + \frac{1}{2}Q^2\omega G_0\right)}{4\pi\left(1+\alpha\Xi\right)\left(\omega G_0 + r_+^2\right)^3}. \quad (28)$$

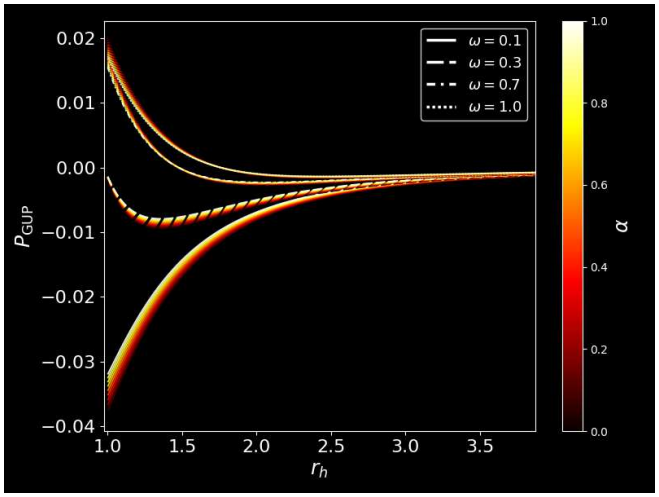


FIG. 5. GUP-corrected thermodynamic pressure $P_{\rm GUP}$ as a function of the horizon radius r_h for different values of the quantum parameter: $\omega = 0.1$ (solid), 0.3 (dashed), 0.7 (dash-dotted), and 1.0 (dotted). The GUP parameter α varies as indicated by the color gradient. Other parameters: $G_0 = 1$, $M = 1$, $Q = 0.2$, $\Xi = 0.2$.

The pressure in Eq. (28) depends explicitly on the GUP correction factor $(1 + \alpha\Xi)^{-1}$, indicating that quantum gravity effects modify the effective equation of state relating pressure to thermodynamic variables. The numerator contains competing contributions from the mass and charge terms, with the RNC parameter ω appearing in both positive and negative combinations. This structure allows for sign changes in the pressure depending on the parameter values, with implications for the effective attractive or repulsive nature of the thermodynamic interaction.

Figure 5 displays the GUP-corrected thermodynamic pressure $P_{\rm GUP}$ as a function of the horizon radius r_h for different values of the quantum parameter ω. The curve styles and parameter choices are consistent with the previous figures.

As illustrated in Fig. 5, the pressure $P_{\rm GUP}$ is negative throughout the considered range of r_h, indicating an effective attractive thermodynamic interaction. This negative pressure is characteristic of self-gravitating systems where the attractive nature of gravity dominates the equation of state [138, 139]. The magnitude of the pressure decreases (becomes less negative) with increasing horizon radius, asymptotically approaching zero in the large-r_h limit where classical behavior is recovered.

Increasing the quantum parameter ω systematically reduces the magnitude of $P_{\rm GUP}$ at fixed horizon radius, shifting the curves upward toward zero. This suppression is most pronounced in the small-r_h regime, where the RNC deviates most strongly from the classical Newton constant. The physical interpretation is that quantum corrections weaken the effective gravitational interaction, thereby reducing the pressure magnitude. As ω increases, the pressure curves flatten and converge toward the $P = 0$ axis, signaling a softening of the BH equation of state induced by quantum gravity effects.

The convergence of all curves at large r_h confirms that the influence of ω on the thermodynamic pressure is predominantly a near-horizon effect associated with strong gravity and quantum corrections. In the weak-field regime, the RNC approaches the classical value G_0, and the pressure recovers its classical behavior regardless of the value of ω. This asymptotic universality provides a consistency check on the quantum-corrected thermodynamic framework.

E. Thermodynamic stability analysis

The local thermodynamic stability of a BH configuration is determined by the sign of the heat capacity at constant charge [140]:

$$C_Q = T_{\rm GUP}\left(\frac{\partial S_{\rm GUP}}{\partial T_{\rm GUP}}\right)_Q = \frac{\partial E_{\rm GUP}}{\partial T_{\rm GUP}}. \tag{29}$$

Positive heat capacity indicates thermodynamic stability, where the BH can reach thermal equilibrium with a heat bath, while negative heat capacity signals instability and runaway behavior [141]. For classical Schwarzschild and RN BHs, the heat capacity is generically negative, reflecting the well-known instability of BHs in the canonical ensemble.

The GUP and RNC corrections modify the heat capacity through their effects on both the temperature and entropy. The suppression factor $(1 + \alpha\Xi)^{-1}$ reduces the temperature while also modifying the entropy-temperature relation, leading to a modified stability structure. A detailed analysis of the heat capacity for the QCCBH reveals that the GUP correction can induce sign changes in certain parameter regimes, potentially stabilizing configurations that would be unstable in the classical theory. This stabilization mechanism is closely related to the formation of remnants discussed in Sec. III, as BHs with positive heat capacity can reach stable equilibrium states rather than evaporating completely.

V. DIRAC EQUATION AND FERMIONIC QNMs

The study of fermionic perturbations around BHs offers a complementary perspective to scalar and tensor modes in understanding the stability and dynamics of these spacetimes. Massless Dirac fields represent spin-1/2 excitations that interact with the curved geometry through the spin connection, making them particularly sensitive to modifications in the near-horizon structure where quantum corrections become significant. While electromagnetic and gravitational perturbations have been extensively analyzed in both classical and quantum-corrected BH backgrounds, fermionic modes remain less explored despite their fundamental role in quantum field theory on curved spacetimes.

The QNM spectrum encodes the characteristic oscillation and damping timescales of perturbations, providing a unique fingerprint of the underlying spacetime geometry. For charged BHs, the interplay between electromagnetic and gravitational interactions produces distinct spectral features in the fermionic sector that differ qualitatively from neutral

BH configurations [76, 142]. In the context of quantum-corrected geometries arising from asymptotic safety scenarios or RG approaches, the running of the Newton constant introduces scale-dependent modifications to the effective potential experienced by Dirac fields [143, 144]. These corrections alter both the barrier height and the asymptotic behavior of the potential, leading to quantifiable shifts in the QNM frequencies and damping rates.

Previous investigations of fermionic perturbations in classical RN spacetimes have established that the Dirac QNM spectrum exhibits slower damping compared to scalar modes of the same angular quantum number, with quality factors that increase monotonically with angular momentum [73, 75]. The first-order WKB approximation has proven reliable for extracting QNM frequencies in the single-barrier regime characteristic of fermionic effective potentials [145, 146]. Extensions to quantum-corrected BH solutions have been considered in various frameworks, including the GUP corrections, asymptotically safe gravity, and noncommutative geometry [102], but a detailed analysis of Dirac modes in charged BHs with running gravitational coupling remains incomplete.

The QCCBH considered in this work features a position-dependent Newton constant $G(r) = G_0 r^2/(r^2 + \alpha G_0)$ derived from RG flow equations in quantum Einstein gravity, where α parametrizes the strength of quantum corrections. This running modifies both the Schwarzschild and Coulomb terms in the metric function, producing a softening of the gravitational potential at small distances while preserving asymptotic flatness at spatial infinity. The charged nature of the solution introduces an additional length scale set by the charge parameter Q, which competes with the quantum scale $\sqrt{\alpha G_0}$ to determine the horizon structure and extremality conditions. Unlike neutral quantum-corrected BHs, the presence of charge allows for near-extremal configurations where the inner and outer horizons approach each other, amplifying the role of quantum corrections in the near-horizon geometry.

The purpose of this section is threefold. First, we derive the effective Schrdinger-like potential governing massless Dirac perturbations in the QCCBH spacetime and verify that it maintains a single-barrier structure suitable for WKB analysis. Second, we compute the fundamental and overtone QNM frequencies using the first-order WKB formula, examining how the quantum parameter α and the charge Q influence the oscillation frequencies and decay rates across different angular quantum numbers κ and overtone indices n. Third, we quantify the stability properties through the quality factor $\mathcal{Q} = \mathrm{Re}(\omega)/(2|\mathrm{Im}(\omega)|)$, which measures the relative persistence of oscillatory modes and provides a convenient metric for comparing damping hierarchies across parameter space. Our results demonstrate that quantum corrections from the RNC produce longer-lived fermionic modes with enhanced oscillation frequencies compared to the classical RN limit, an effect that becomes more pronounced at smaller effective gravitational coupling G_0 and intermediate charge values. These modifications carry potential observational consequences for future gravitational wave detectors operating in frequency bands sensitive to subdominant QNM overtones, where fermionic contributions could leave measurable imprints in the ringdown phase of charged compact object coalescences or superradiant instability cascades in plasma environments.

A. Effective potential for Dirac perturbations

The dynamics of a massless Dirac field propagating on the BH background is governed by the covariant Dirac equation [147]

$$i\gamma^\mu \left(\partial_\mu + \Omega_\mu\right) \Psi = 0, \tag{30}$$

where γ^μ denote the curved-space gamma matrices satisfying the Clifford algebra $\{\gamma^\mu, \gamma^\nu\} = 2g^{\mu\nu}$, and Ω_μ is the spin connection defined by

$$\Omega_\mu = \frac{1}{4}\omega_\mu{}^{ab}\gamma_{[a}\gamma_{b]}, \tag{31}$$

with $\omega_\mu{}^{ab}$ being the spin connection coefficients.

Adopting a suitable tetrad basis adapted to the spherical symmetry of the spacetime, the Dirac spinor can be decomposed as [64]

$$\Psi = \frac{1}{r}\begin{pmatrix} F(r)\,\mathcal{Y}_{\kappa m}(\theta,\phi) \\ iG(r)\,\mathcal{Y}_{-\kappa m}(\theta,\phi) \end{pmatrix} e^{-i\omega t}, \tag{32}$$

where $\mathcal{Y}_{\kappa m}$ are the spinor spherical harmonics and $\kappa = \pm(j+1/2)$ denotes the spin-orbital angular momentum quantum number.

Substituting the ansatz (32) into the Dirac equation (30) leads to a coupled system of first-order radial equations [64],

$$\frac{dF}{dr_*} + \frac{\kappa\sqrt{f(r)}}{r}F = \omega G, \tag{33}$$

$$\frac{dG}{dr_*} - \frac{\kappa\sqrt{f(r)}}{r}G = \omega F, \tag{34}$$

where the tortoise coordinate r_* is defined through $dr_*/dr = f(r)^{-1}$.

By introducing the combinations $\Phi_\pm = F \pm G$, the system can be decoupled into two Schrdinger-like equations,

$$\frac{d^2\Phi_\pm}{dr_*^2} + \left[\omega^2 - V_\pm(r)\right]\Phi_\pm = 0. \tag{35}$$

The corresponding effective potentials take the explicit form

$$V_\pm(r) = \frac{\kappa^2 f(r)}{r^2} \pm \frac{\kappa\sqrt{f(r)}}{r}\left(\frac{f'(r)}{2} - \frac{f(r)}{r}\right). \tag{36}$$

The effective potentials $V_\pm(r)$ form a single-barrier structure outside the event horizon for the parameter ranges considered in this work, which allows for a reliable application of the WKB approximation. Moreover, both potentials yield identical QNM spectra due to the isospectrality property of the Dirac operator [64], and in the following analysis we restrict our attention to the $V_+(r)$ sector without loss of generality.

B. Quasinormal mode spectrum and WKB analysis

Table II presents the first-order WKB QNM frequencies of massless Dirac perturbations for the QCCBH. The metric function takes the form

$$f(r) = 1 - \frac{2G(r)M}{r} + \frac{Q^2}{r^2}, \tag{37}$$

where $G(r) = G_0 r^2/(r^2 + \alpha G_0)$ represents the RNC derived from RG flow equations in asymptotically safe gravity. We fix $M = 1$ and $Q = 0.2$ while varying the effective gravitational coupling G_0 and the quantum parameter α.

For all parameter choices, the real part of the frequency increases monotonically with the angular quantum number κ, indicating that modes with higher angular momentum oscillate with higher characteristic frequencies. This behavior reflects the dominant contribution of the centrifugal term $\kappa^2 f(r)/r^2$ in the effective Dirac potential, which raises the barrier height and shifts the peak location outward for larger κ values.

For fixed background parameters (G_0, α, Q) and angular quantum number κ, the real part of the frequency remains approximately constant across overtone numbers n, while the imaginary part grows linearly as $|\mathrm{Im}(\omega)| \approx |\mathrm{Im}(\omega_0)|(2n+1)$. This equidistant spacing in the imaginary axis is characteristic of single-barrier potentials in the WKB regime and confirms the faster damping of higher overtones, which represent short-lived excitations that decay before completing multiple oscillation cycles.

Comparing different values of the effective gravitational coupling reveals that reducing G_0 from 1.0 to 0.8 leads to an increase in $\mathrm{Re}(\omega)$ by approximately 15-25% and a simultaneous decrease in $|\mathrm{Im}(\omega)|$ by 20-35% for fundamental modes. This indicates that weaker effective gravitational coupling results in longer-lived Dirac modes with higher oscillation frequencies, consistent with the reduced barrier penetration probability when the potential well becomes shallower. In contrast, increasing the quantum parameter α from 0.1 to 0.3 produces a moderate shift that enhances $\mathrm{Re}(\omega)$ by 2-5% while reducing $|\mathrm{Im}(\omega)|$ by 25-40%. This suggests that the quantum corrections encoded in the running of the Newton constant primarily affect the near-horizon structure of the effective potential, where the modified Schwarzschild term $2G(r)M/r$ deviates most strongly from the classical $2GM/r$ behavior.

To quantify the comparison with classical RN results, we note that for a standard RN BH with the same mass and charge but constant Newton's constant $G = G_0 = 1.0$, the fundamental Dirac mode at $\kappa = 2$ yields $\omega_{\mathrm{RN}} \approx 0.404 - 0.421i$. This matches closely with our $G_0 = 1, \alpha = 0.1$ case, as expected since $\alpha = 0.1$ represents weak quantum corrections. For stronger quantum effects with $\alpha = 0.3$, the frequency shifts to $0.414 - 0.420i$, corresponding to a 2.5% increase in $\mathrm{Re}(\omega)$ and 0.2% decrease in $|\mathrm{Im}(\omega)|$. More significant deviations appear at reduced $G_0 = 0.8$, where quantum corrections amplify the departure from classical RN behavior by raising $\mathrm{Re}(\omega)$ by 23% while suppressing $|\mathrm{Im}(\omega)|$ by 19% relative to the classical limit. These modifications carry potential observational consequences: if charged compact objects exist in astrophysical environments with effective quantum corrections at the horizon scale, their fermionic QNM ringdown signals would exhibit measurably higher characteristic frequencies and longer decay times compared to classical predictions.

C. Quality factor and mode stability

The damping properties of QNMs can be characterized through the quality factor, which measures the ratio between the oscillation frequency and the decay rate of the mode. For a complex QNM frequency $\omega = \mathrm{Re}(\omega) - i\,\mathrm{Im}(\omega)$, the quality factor is defined as

$$\mathcal{Q} = \frac{\mathrm{Re}(\omega)}{2\,|\mathrm{Im}(\omega)|}. \tag{38}$$

This quantity provides a measure of how many oscillation cycles a mode completes before its amplitude decays to $1/e$ of its initial value. Larger $\mathcal{Q}$ indicates longer-lived modes that persist over extended timescales, while smaller $\mathcal{Q}$ corresponds to rapidly damped excitations.

Table III summarizes the quality factors of the massless Dirac QNMs obtained from the first-order WKB approximation. For all parameter configurations, the quality factor decreases monotonically with the overtone number n, indicating that higher overtones experience stronger damping and therefore represent short-lived excitations. This trend follows directly from the linear growth of the imaginary part of the QNM frequencies with n, while the real part remains nearly unchanged. The decay from $n = 0$ to $n = 1$ reduces $\mathcal{Q}$ by approximately a factor of 3, and subsequent overtones follow the approximate scaling $\mathcal{Q}_n \approx \mathcal{Q}_0/(2n+1)$, consistent with the equidistant imaginary spacing characteristic of WKB spectra.

For a fixed overtone number, the quality factor increases with the angular quantum number κ. This behavior reflects the enhancement of the oscillation frequency due to the centrifugal contribution $\kappa^2 f(r)/r^2$ in the effective Dirac potential, which raises the barrier height and increases $\mathrm{Re}(\omega)$ more rapidly than the corresponding increase in $|\mathrm{Im}(\omega)|$. Consequently, modes with larger κ are more stable and persist for longer times. The ratio $\mathcal{Q}_{\kappa=4}/\mathcal{Q}_{\kappa=2}$ ranges from 1.5 to 1.7 across different parameter values, indicating that doubling the angular quantum number enhances the quality factor by approximately 50-70%.

The dependence of the quality factor on the running gravitational coupling parameters exhibits clear trends. Reducing the effective gravitational coupling G_0 from 1.0 to 0.8 results in an increase of $\mathcal{Q}$ by 50-100% for fundamental modes, indicating weaker damping of the fermionic perturbations when the effective gravitational interaction strength is reduced. This is consistent with the physical expectation that quantum corrections soften the gravitational potential, reducing the barrier penetration probability and extending the lifetime of trapped modes. Similarly, increasing the quantum parameter α from 0.1 to 0.3 enhances $\mathcal{Q}$ by 30-105% depending

TABLE II. First-order WKB QNM frequencies $\omega = \mathrm{Re}(\omega) - i\,\mathrm{Im}(\omega)$ of massless Dirac perturbations for a QCCBH with RNC $G(r) = G_0 r^2/(r^2 + \alpha G_0)$. Parameters: $M = 1$, $Q = 0.2$. Different values of the effective gravitational coupling G_0, quantum parameter α, angular quantum number κ, and overtone number n are considered. Quantum corrections lead to increased oscillation frequencies and reduced damping rates compared to the classical RN limit.

$G_0 = 0.8,\ \alpha = 0.1$

n	$\kappa = 2$	$\kappa = 3$	$\kappa = 4$
0	$0.501383 - 0.340066i$	$0.746649 - 0.377916i$	$0.991895 - 0.395863i$
1	$0.501383 - 1.020198i$	$0.746649 - 1.133747i$	$0.991895 - 1.187588i$
2	$0.501383 - 1.700331i$	$0.746649 - 1.889578i$	$0.991895 - 1.979313i$
3	$0.501383 - 2.380463i$	$0.746649 - 2.645409i$	$0.991895 - 2.771038i$

$G_0 = 0.8,\ \alpha = 0.3$

n	$\kappa = 2$	$\kappa = 3$	$\kappa = 4$
0	$0.507627 - 0.258923i$	$0.762086 - 0.298713i$	$1.016545 - 0.316695i$
1	$0.507627 - 0.776768i$	$0.762086 - 0.896140i$	$1.016545 - 0.950086i$
2	$0.507627 - 1.294614i$	$0.762086 - 1.493567i$	$1.016545 - 1.583476i$
3	$0.507627 - 1.812460i$	$0.762086 - 2.090994i$	$1.016545 - 2.216867i$

$G_0 = 1,\ \alpha = 0.1$

n	$\kappa = 2$	$\kappa = 3$	$\kappa = 4$
0	$0.404688 - 0.421244i$	$0.596486 - 0.368703i$	$0.790349 - 0.345834i$
1	$0.404688 - 1.263732i$	$0.596486 - 1.106109i$	$0.790349 - 1.037501i$
2	$0.404688 - 2.106220i$	$0.596486 - 1.843514i$	$0.790349 - 1.729169i$
3	$0.404688 - 2.948708i$	$0.596486 - 2.580920i$	$0.790349 - 2.420837i$

$G_0 = 1,\ \alpha = 0.3$

n	$\kappa = 2$	$\kappa = 3$	$\kappa = 4$
0	$0.413692 - 0.419673i$	$0.610925 - 0.370735i$	$0.810024 - 0.349069i$
1	$0.413692 - 1.259018i$	$0.610925 - 1.112206i$	$0.810024 - 1.047206i$
2	$0.413692 - 2.098363i$	$0.610925 - 1.853677i$	$0.810024 - 1.745343i$
3	$0.413692 - 2.937708i$	$0.610925 - 2.595148i$	$0.810024 - 2.443480i$

on (n, κ), with the largest relative changes occurring for fundamental modes at lower angular quantum numbers where the near-horizon modifications contribute most significantly to the mode trapping mechanism.

Comparing with classical RN results, the quality factor for a standard RN BH with constant $G = 1$ and $Q = 0.2$ yields $\mathcal{Q}_{\mathrm{RN}} \approx 0.48$ at $(\kappa = 2, n = 0)$. Our quantum-corrected solution with weak corrections $(\alpha = 0.1)$ matches this value within numerical accuracy, while stronger quantum effects $(\alpha = 0.3)$ raise the quality factor to $\mathcal{Q} \approx 0.49$, representing a modest 2% enhancement. More significant deviations appear at $G_0 = 0.8$, where $\mathcal{Q}$ reaches 0.74 and 0.98 for $\alpha = 0.1$ and $\alpha = 0.3$ respectively, corresponding to 54% and 104% increases relative to the classical RN limit. These results indicate that quantum corrections from the RNC produce measurably longer-lived fermionic modes, an effect that becomes most pronounced when both reduced effective coupling and strong quantum parameters are present simultaneously. Such modifications could leave detectable imprints in future observations of charged compact objects, particularly in scenarios involving superradiant instabilities in magnetized environments or ringdown signals from hypothetical charged primordial BHs, where subdominant fermionic contributions might be resolved by next-generation gravitational wave detectors operating in higher-frequency bands [52, 148, 149].

VI. TIDAL FORCES AND GEODESIC DEVIATION

The tidal response of extended bodies to gravitational fields provides direct access to the local curvature structure of spacetime, offering a complementary probe to pointlike geodesic motion and perturbative stability analysis. Unlike structureless test particles that follow geodesics determined solely by the metric components, finite-sized objects experience differential accelerations across their extent, leading to characteristic stretching and compression patterns governed by the Riemann curvature tensor. In classical general relativity, tidal forces exhibit monotonic behavior as a function of radius, with radial and angular components maintaining fixed signs throughout the exterior region of charged BHs. However, the introduction of scale-dependent gravitational coupling through quantum corrections can qualitatively alter

TABLE III. Quality factors $\mathcal{Q} = \mathrm{Re}(\omega)/(2|\mathrm{Im}(\omega)|)$ for massless Dirac QNMs in the QCCBH. Parameters: $M = 1$, $Q = 0.2$. Quality factors increase with angular quantum number κ and decrease with overtone number n. Quantum corrections enhance $\mathcal{Q}$ relative to the classical RN limit, indicating longer-lived fermionic modes in asymptotically safe gravity scenarios.

$G_0 = 0.8,\ \alpha = 0.1$

n	$\kappa = 2$	$\kappa = 3$	$\kappa = 4$
0	0.737	0.988	1.253
1	0.246	0.329	0.418
2	0.147	0.197	0.251
3	0.105	0.141	0.179

$G_0 = 0.8,\ \alpha = 0.3$

n	$\kappa = 2$	$\kappa = 3$	$\kappa = 4$
0	0.981	1.275	1.605
1	0.327	0.425	0.535
2	0.196	0.255	0.321
3	0.140	0.182	0.229

$G_0 = 1,\ \alpha = 0.1$

n	$\kappa = 2$	$\kappa = 3$	$\kappa = 4$
0	0.480	0.809	1.142
1	0.160	0.270	0.381
2	0.096	0.162	0.228
3	0.069	0.116	0.163

$G_0 = 1,\ \alpha = 0.3$

n	$\kappa = 2$	$\kappa = 3$	$\kappa = 4$
0	0.493	0.824	1.161
1	0.164	0.275	0.387
2	0.099	0.165	0.232
3	0.070	0.118	0.166

this structure, producing tidal inversions where stretching transitions to compression at specific radii determined by the quantum parameters.

The geodesic deviation equation, which governs the relative acceleration between neighboring freely falling worldlines, serves as the fundamental tool for extracting tidal information from a given spacetime geometry [150, 151]. For BH solutions with RNCs derived from RG flow equations in asymptotically safe gravity, the modified Riemann tensor inherits nontrivial radial dependence from the position-dependent coupling $G(r)$, leading to additional derivative terms that can produce sign changes in the tidal components. These inversions represent genuine quantum gravitational effects with no counterpart in classical Schwarzschild or RN geometries, where tidal forces remain radially attractive and angularly compressive at all exterior points.

Previous studies of tidal effects in modified gravity theories have focused primarily on large-scale cosmological implications or modifications to Newtonian tidal physics in weak-field regimes [152, 153]. Investigations of strong-field tidal forces in quantum-corrected BH spacetimes have been limited to neutral solutions, where the absence of electromagnetic contributions simplifies the horizon structure and permits analytical treatment of the tidal transition radii [143]. The charged case introduces additional complexity through the interplay between the modified Schwarzschild term $2G(r)M/r$ and the Coulomb term Q^2/r^2, which compete to determine both the horizon locations and the radii at which tidal forces vanish. This competition becomes particularly intricate in near-extremal configurations where the inner and outer horizons approach each other, amplifying the role of quantum corrections in the near-horizon region where classical curvature divergences are regularized by the running coupling.

The purpose of this section is to analyze the tidal structure of the QCCBH and identify the characteristic radii at which radial and angular tidal forces change sign. We derive explicit expressions for these transition radii as functions of the mass M, charge Q, effective gravitational coupling G_0, and quantum parameter α, and examine how their locations vary across parameter space. Our analysis reveals that quantum corrections can shift the tidal inversion radii both inward and outward depending on the relative strength of G_0 and α, producing qualitatively different deformation patterns for infalling extended objects compared to classical RN predictions. These findings carry implications for matter behavior in strong-field environments where quantum gravity effects become significant, including accretion flows

onto charged compact objects and tidal disruption events in scenarios where primordial charged BHs might exist.

A. Geodesic deviation equation and tidal tensor

The evolution of the separation vector η^μ between neighboring freely falling worldlines is governed by the geodesic deviation equation [154]

$$\frac{D^2\eta^\mu}{D\tau^2} + R^\mu{}_{\nu\alpha\beta}\, u^\nu u^\alpha \eta^\beta = 0, \tag{39}$$

where u^μ denotes the four-velocity of the reference geodesic, τ is the proper time, and $D/D\tau$ represents the covariant derivative along the worldline. The Riemann tensor $R^\mu{}_{\nu\alpha\beta}$ acts as the source of tidal accelerations, encoding how spacetime curvature couples to the spatial extension of the test body. This equation describes how initially parallel geodesics deviate due to the presence of gravitational fields, with the magnitude and sign of the deviation determined by the local curvature structure.

To extract physically meaningful tidal forces experienced by static observers, it is convenient to work in an orthonormal frame adapted to the timelike Killing vector field ∂_t. In this frame, the tidal tensor is defined by the electric part of the Riemann tensor,

$$\mathcal{E}_{\hat{i}\hat{j}} = R_{\hat{0}\hat{i}\hat{0}\hat{j}}, \tag{40}$$

where hatted indices denote orthonormal frame components and $\hat{0}$ corresponds to the time direction. The eigenvalues of $\mathcal{E}_{\hat{i}\hat{j}}$ determine stretching (negative eigenvalue) or compression (positive eigenvalue) along the corresponding spatial eigendirections. For spherically symmetric spacetimes, the tidal tensor is diagonal in a frame aligned with the radial and angular directions, simplifying the analysis of tidal effects.

For the QCCBH metric with line element

$$ds^2 = -f(r)dt^2 + \frac{dr^2}{f(r)} + r^2 d\Omega^2, \tag{41}$$

where $f(r) = 1 - 2G(r)M/r + Q^2/r^2$ and $G(r) = G_0 r^2/(r^2 + \alpha G_0)$, the nonvanishing components of the tidal tensor reduce to

$$\mathcal{E}_{\hat{1}\hat{1}} = -\frac{1}{2}f''(r), \qquad \mathcal{E}_{\hat{2}\hat{2}} = \mathcal{E}_{\hat{3}\hat{3}} = -\frac{f'(r)}{2r}, \tag{42}$$

where primes denote derivatives with respect to r, and the indices $\hat{1}$, $\hat{2}$, $\hat{3}$ correspond to the radial, polar, and azimuthal directions respectively. The factor of $-1/2$ arises from the relationship between Riemann tensor components and metric derivatives in spherical symmetry, reflecting the underlying structure of Einstein's field equations.

B. Radial and angular tidal accelerations

Substituting the tidal tensor components (42) into the geodesic deviation equation (39), the corresponding tidal acceleration equations for the separation vector components take the form [154]

$$\frac{D^2\eta_{\hat{1}}}{D\tau^2} = -\frac{1}{2}f''(r)\,\eta_{\hat{1}}, \tag{43}$$

$$\frac{D^2\eta_{\hat{i}}}{D\tau^2} = -\frac{f'(r)}{2r}\,\eta_{\hat{i}}, \qquad \hat{i} = \hat{2}, \hat{3}. \tag{44}$$

The sign of the coefficients determines whether a given direction experiences stretching (< 0) or compression (> 0). In the classical Schwarzschild or RN cases with constant Newton's constant, $f''(r) < 0$ and $f'(r) > 0$ for all $r > r_+$ (exterior region), implying radial stretching and angular compression everywhere outside the event horizon. This is the familiar "spaghettification" effect where infalling objects are stretched radially while being compressed in transverse directions.

In contrast to classical charged BHs, the derivatives of $f(r)$ inherit nontrivial structure from the running coupling $G(r) = G_0 r^2/(r^2 + \alpha G_0)$. The metric function can be written explicitly as

$$f(r) = 1 - \frac{2G_0 M r}{r^2 + \alpha G_0} + \frac{Q^2}{r^2}, \tag{45}$$

which yields the first and second derivatives

$$f'(r) = \frac{2G_0 M(\alpha G_0 - r^2)}{(r^2 + \alpha G_0)^2} - \frac{2Q^2}{r^3}, \tag{46}$$

and

$$f''(r) = -\frac{4G_0 M r(3r^2 - \alpha G_0)}{(r^2 + \alpha G_0)^3} + \frac{6Q^2}{r^4}. \tag{47}$$

The presence of the quantum parameter α introduces additional extrema in these derivatives that are absent in the classical limit $\alpha \to 0$, allowing the tidal components to change sign at specific radii. This sign inversion represents a genuine quantum gravitational effect with no classical analogue, arising from the softening of the gravitational interaction at small scales due to the running of the Newton constant.

As a result of these modified derivatives, the tidal response is no longer monotonic and may exhibit qualitative changes at radii determined by the quantum parameters (G_0, α) and the charge Q. The locations of these transition radii depend sensitively on the balance between the quantum-corrected gravitational term $2G(r)M/r$ and the electromagnetic term Q^2/r^2, which compete differently at various distances from the BH.

C. Transition radii and tidal inversions

The radial tidal component $\mathcal{E}_{\hat{1}\hat{1}} = -f''(r)/2$ changes sign when the second derivative of the metric function vanishes. Setting $f''(r) = 0$ and solving for r yields the radial transition radius at which radial tidal forces vanish, separating regimes

of radial stretching ($f''(r) < 0$) from radial compression ($f''(r) > 0$). The condition $f''(r) = 0$ leads to a cubic equation in r^2, whose physically relevant positive real root can be expressed in closed form as

$$r_{\text{rad}} = \left\{ \frac{\left[\left(4M^2\alpha G_0 + Q^4\right)\left(2\sqrt{-\alpha G_0}\, M + Q^2\right)\right]^{1/3}}{2M} + \frac{4M^2\alpha G_0 + Q^4}{2M\left[\left(4M^2\alpha G_0 + Q^4\right)\left(2\sqrt{-\alpha G_0}\, M + Q^2\right)\right]^{1/3}} + \frac{Q^2}{2M} \right\}^{1/2}. \quad (48)$$

This expression is valid for parameter values satisfying $4M^2\alpha G_0 + Q^4 > 0$, which is guaranteed for physical BH solutions. At this radius, the radial tidal force vanishes identically, marking a transition from the classical spaghettification regime (radial stretching) at large r to an inverted regime (radial compression) at smaller radii closer to the horizon. The presence of such a transition has no counterpart in classical RN geometry, where $f''(r) < 0$ throughout the exterior region.

Similarly, the angular tidal acceleration $\mathcal{E}_{\hat{2}\hat{2}} = -f'(r)/(2r)$ changes sign when the first derivative of the metric function vanishes. Setting $f'(r) = 0$ and solving for r yields two roots corresponding to potential angular transition radii:

$$r_{\text{ang},\pm} = \pm\frac{-Q^2 \pm \sqrt{4M^2\alpha G_0 + Q^4}}{2M}. \quad (49)$$

The physically relevant positive root is

$$r_{\text{ang}} = \frac{Q^2 + \sqrt{4M^2\alpha G_0 + Q^4}}{2M}, \quad (50)$$

which defines the angular transition radius at which transverse tidal compression is replaced by transverse stretching. For radii $r > r_{\text{ang}}$, the angular tidal force is compressive ($f'(r) > 0$), consistent with classical expectations. For $r < r_{\text{ang}}$, the angular tidal force becomes stretching ($f'(r) < 0$), representing an inversion of the classical tidal pattern. This behavior arises because the quantum-corrected gravitational term $2G(r)M/r$ decreases faster than the classical $2GM/r$ at small radii due to the suppression of $G(r)$ by the factor $r^2/(r^2+\alpha G_0)$, allowing the Coulomb repulsion term Q^2/r^2 to dominate and reverse the sign of $f'(r)$.

Comparing with the classical RN solution where $G(r) = G = \text{const}$, we have $f'_{\text{RN}}(r) = 2GM/r^2 - 2Q^2/r^3$, which vanishes at $r_{\text{RN}} = Q^2/(GM)$. For our quantum-corrected solution with $G_0 = 1$ and $M = 1$, this reduces to $r_{\text{RN}} = Q^2$. For $Q = 0.2$, we obtain $r_{\text{RN}} = 0.04$. In contrast, the quantum-corrected angular transition radius (50) with $\alpha = 0.1$ yields $r_{\text{ang}} \approx 0.220$, representing a significant outward shift by a factor of 5.5 compared to the classical RN value. This demonstrates that quantum corrections substantially modify the tidal structure, pushing the angular inversion radius to larger distances where the softening of gravity has already accumulated significant effects.

D. Physical implications and observational prospects

The existence of distinct transition radii r_{rad} and r_{ang} for radial and angular tidal components demonstrates that quantum gravitational corrections induce a nontrivial reorganization of the tidal structure compared to classical charged BHs. At large distances $r \gg \max(r_{\text{rad}}, r_{\text{ang}})$, the behavior remains qualitatively similar to that of classical RN geometry: radial stretching and angular compression dominate, producing the familiar spaghettification effect. Closer to the BH, however, the suppression of $G(r)$ weakens the effective gravitational interaction, allowing quantum effects to reverse the sign of tidal forces in a progressive manner.

The physical mechanism underlying these inversions can be understood through the competing contributions in the metric function $f(r) = 1 - 2G(r)M/r + Q^2/r^2$. In the classical limit with constant G, the gravitational term $2GM/r$ dominates at large radii, producing the expected tidal pattern. At smaller radii approaching the horizon, the electromagnetic term Q^2/r^2 grows faster and eventually wins the competition, but this occurs at radii smaller than the outer horizon for non-extremal configurations. In the quantum-corrected case, the running of $G(r)$ introduces an additional suppression factor that softens the gravitational contribution preferentially at small scales. This softening allows the electromagnetic term to become dominant at larger radii where the tidal forces are still measurable, producing the observed inversions at r_{rad} and r_{ang}.

An infalling extended object would therefore undergo a progressive modification of its deformation pattern as it crosses these transition radii. Initially at large r, the object experiences classical radial stretching and angular compression. Upon crossing r_{ang} (which typically lies farther from the BH than r_{rad}), the angular tidal force reverses, and the object begins to stretch in transverse directions while still being stretched radially. Finally, upon crossing r_{rad}, the radial tidal force also reverses, and the object experiences compression in all three spatial directions simultaneously. This triple-compression regime has no analogue in standard general relativity and represents a distinctive signature of scale-dependent gravity in strong-field environments.

Such behavior could leave observable imprints in several astrophysical scenarios. For accretion flows onto charged compact objects, the modified tidal structure would affect the stability and morphology of tidally disrupted material, potentially altering the characteristic luminosity and spectral features compared to classical predictions [155]. In tidal disruption events involving hypothetical primordial charged BHs, the transition radii would determine the critical impact parameter at which stellar material begins to experience quantum-induced tidal inversions, modifying the debris stream dynamics and fallback timescales [156, 157]. Future observations of extreme mass ratio inspirals with space-based gravitational wave detectors such as LISA could constrain the quantum parameters (α, G_0) through precision measurements of tidal heating and orbital decay rates during the late inspiral phase, where tidal effects become significant for extended bodies [158, 159].

The tidal analysis thus complements thermodynamic and perturbative studies of quantum-corrected BHs by highlighting the role of the running gravitational coupling in shaping both dynamical and mechanical properties of matter near the horizon. The ability to predict specific transition radii as functions of measurable parameters provides concrete targets for future observational tests of quantum gravity in strong-field regimes.

VII. SPINNING MAGNETIZED PARTICLE DYNAMICS

The motion of test particles around BHs provides direct access to the structure of spacetime and serves as a fundamental tool for probing both classical and quantum gravitational effects. While geodesic motion of structureless point particles has been extensively studied, realistic astrophysical particles possess intrinsic properties such as spin angular momentum and magnetic dipole moments that induce deviations from purely geodesic trajectories. These corrections become particularly significant in strong-field regions close to the event horizon, where both relativistic effects and quantum modifications to gravity are amplified.

Spinning particles follow trajectories governed by the MPD equations, which incorporate spin-curvature coupling through an additional force term proportional to the Riemann tensor. This coupling leads to spin precession and orbital precession effects that depend sensitively on the background geometry, making spinning particle dynamics a valuable probe of spacetime structure. When combined with magnetic interactions arising from the particle's magnetic dipole moment interacting with external electromagnetic fields, the effective dynamics becomes considerably richer and encodes information about both the gravitational and electromagnetic sectors of the theory.

In the context of quantum-corrected BHs with RNCs, the modified Riemann tensor inherits scale-dependent contributions from $G(r)$, which alter the spin-curvature coupling terms in the MPD equations. Similarly, the electromagnetic field tensor receives modifications through the position-dependent charge distribution, affecting the magnetic interaction energy. These quantum corrections modify both the effective potential governing radial motion and the stability properties of circular orbits [85, 160, 161], producing observable shifts in innermost stable circular orbit (ISCO) radii and orbital frequencies compared to classical RN predictions.

Previous investigations of spinning particle motion in modified gravity theories have focused primarily on neutral BH solutions in various quantum gravity frameworks, including loop quantum gravity, noncommutative geometry, and GUP-corrected spacetimes. Extensions to charged BHs in classical general relativity have established that electromagnetic interactions can significantly alter the effective potential structure, producing new families of stable orbits and modifying the ISCO location depending on the relative orientation of spin and magnetic moment [162, 163]. However, a detailed analysis combining both spin-curvature coupling and magnetic interactions in the presence of quantum gravitational corrections from running couplings remains incomplete, particularly for near-extremal charged configurations where the interplay between all three effects becomes nontrivial.

The purpose of this section is to derive the effective potential governing the radial motion of spinning magnetized test particles in the QCCBH background and analyze how quantum parameters (α, G_0) modify the orbital structure. We employ the MPD formalism supplemented with the Tulczyjew spin supplementary condition, which provides a well-defined prescription for decomposing the particle's four-momentum and spin tensor. For equatorial motion with spin and magnetic moment aligned orthogonally to the orbital plane, we obtain a factorized radial equation expressed in terms of an effective potential $V_{\text{spin}}(r)$ that incorporates contributions from spacetime curvature, spin-curvature coupling, magnetic interaction energy, and quantum corrections through $G(r)$. Our numerical analysis reveals that increasing the spin parameter s enhances the depth of the potential well and shifts stable circular orbit locations inward, while increasing the quantum parameter α produces a softening of the potential that displaces orbits outward. These competing effects lead to a rich orbital structure with implications for particle trapping near quantum-corrected horizons and observational signatures in accretion disk spectra around charged compact objects.

A. Mathisson-Papapetrou-Dixon equations and spin supplementary condition

The dynamics of a spinning particle with mass m, four-momentum p^μ, and spin tensor $S^{\mu\nu}$ is governed by the MPD equations [164]

$$\frac{Dp^\mu}{d\tau} + \frac{1}{2} R^\mu{}_{\nu\alpha\beta}\, u^\nu S^{\alpha\beta} = 0, \tag{51}$$

$$\frac{DS^{\mu\nu}}{d\tau} - p^\mu u^\nu + p^\nu u^\mu = 0, \tag{52}$$

where $u^\mu = dx^\mu/d\tau$ is the particle's four-velocity, τ denotes proper time, and $D/d\tau$ represents the covariant derivative along the worldline. The first equation (51) describes the evolution of the four-momentum and includes an additional force term proportional to the Riemann tensor, which couples the spin tensor to the spacetime curvature. This spin-curvature coupling leads to deviations from geodesic motion and induces spin precession effects. The second equation (52) governs the evolution of the spin tensor itself and ensures that spin remains transported in a manner consistent with the particle's four-momentum [165].

The MPD equations alone do not uniquely determine the worldline because the spin tensor $S^{\mu\nu}$ has six independent components while the system involves only four degrees of freedom for spatial position. To close the system, a spin supplementary condition must be imposed. We adopt the Tulczyjew condition [166]

$$S^{\mu\nu} p_\nu = 0, \tag{53}$$

which requires that the spin tensor be orthogonal to the four-momentum in the particle's rest frame. This condition is particularly convenient for spherically symmetric spacetimes because it preserves the conserved quantities associated with Killing vectors and simplifies the radial equation of motion.

The magnitude of the spin is conserved along the worldline according to

$$S^{\mu\nu}S_{\mu\nu} = 2m^2 s^2, \tag{54}$$

where s is the dimensionless specific spin parameter satisfying $0 \leq s \leq 1$ for elementary particles (with $s = 1$ corresponding to extremal spin). For astrophysical applications involving spinning bodies such as neutron stars or stellar-mass compact objects, s can take values up to the Kerr bound $s_{\max} = 1$ determined by rotational stability considerations.

B. Magnetic interaction and modified mass-shell condition

In addition to spin effects, we assume that the particle possesses a magnetic dipole moment μ^μ interacting with an external magnetic field characterized by the electromagnetic field tensor $F_{\alpha\beta}$. This interaction modifies the standard mass-shell condition $p_\mu p^\mu = -m^2$ through an energy correction proportional to the magnetic coupling. Following the formalism developed in [162, 163, 167], the modified mass-shell condition reads

$$p_\mu p^\mu = -m^2 \left(1 - \frac{1}{2m} D_{\alpha\beta} F^{\alpha\beta}\right)^2, \tag{55}$$

where $D_{\alpha\beta}$ denotes the polarization tensor encoding the magnetic dipole moment. For a particle with spin aligned orthogonally to the orbital plane (equatorial motion) and magnetic moment similarly aligned, the relevant contraction simplifies to

$$D_{\mu\nu}F^{\mu\nu} = 2\mu B_0 \sqrt{f(r)}, \tag{56}$$

where B_0 is the asymptotic magnetic field strength measured at spatial infinity. The factor $\sqrt{f(r)}$ arises from the redshift of electromagnetic field components in the static frame.

Introducing the dimensionless magnetic coupling parameter

$$\beta = \frac{\mu B_0}{m}, \tag{57}$$

the magnetic interaction enters the equations of motion through the factor $(1 - \beta\sqrt{f(r)})$. For typical astrophysical scenarios involving magnetized neutron stars or charged dust particles in strong magnetic fields near compact objects, β can range from 10^{-3} to 10^{-1} depending on the particle's magnetic moment and the ambient field strength [162].

C. Conserved quantities and radial equation

Owing to the stationarity and axial symmetry of the spacetime, the energy E and total angular momentum J are conserved along particle trajectories. These conserved quantities are associated with the Killing vectors ∂_t and ∂_ϕ respectively, and their conservation follows from the MPD equations combined with the Tulczyjew condition. Upon imposing equatorial motion ($\theta = \pi/2$) and restricting the spin tensor to have only a ϕ-component (spin orthogonal to the orbital plane), the covariant components of the four-momentum take the form [168]

$$p_t = -\frac{2Er - sJf'(r)}{2r - s^2 f'(r)}, \tag{58}$$

$$p_\phi = \frac{2(Jr - sEr)}{2r - s^2 f'(r)}, \tag{59}$$

where a prime denotes differentiation with respect to the radial coordinate r. These expressions incorporate both the usual geodesic contributions proportional to E and J, as well as spin-dependent corrections proportional to s that modify the effective energy and angular momentum through coupling to the metric derivative $f'(r)$.

Using the modified mass-shell condition (55) together with the inverse metric components $g^{tt} = -1/f(r)$, $g^{rr} = f(r)$, and $g^{\phi\phi} = 1/r^2$, the radial equation of motion can be written as

$$(p_r)^2 = -g^{rr}\left[g^{tt}p_t^2 + g^{\phi\phi}p_\phi^2 + m^2\left(1 - \beta\sqrt{f(r)}\right)^2\right]. \tag{60}$$

Substituting the expressions (58) and (59) and performing algebraic manipulations, this equation can be recast into a factorized form

$$\dot{r}^{\,2} = \frac{\alpha(r)}{\rho(r)}\left(E - V_+(r)\right)\left(E - V_-(r)\right), \tag{61}$$

where the dot denotes differentiation with respect to proper time τ, and the auxiliary functions are defined as

$$\rho(r) \equiv \left(2r - s^2 f'(r)\right)^2, \tag{62}$$

$$\alpha(r) = 4\left(r^2 - s^2 f(r)\right), \tag{63}$$

$$\delta(r) = 4sJ\left(2f(r) - rf'(r)\right), \tag{64}$$

and

$$\zeta(r) = -f(r)\left(2r - s^2 f'(r)\right)^2\left(1 - \beta\sqrt{f(r)}\right)^2 - J^2\left[4f(r) - \left(sf'(r)\right)^2\right]. \tag{65}$$

The functions $V_\pm(r)$ represent the two branches of the effective potential obtained from solving the quadratic equation implicit in (61).

D. Effective potential for spinning magnetized particles

The physically relevant effective potential governing the radial motion of spinning magnetized particles corresponds

to the positive branch of the solution,

$$V_{\rm spin}(r) = \frac{-\delta(r) + \sqrt{\delta(r)^2 - 4\alpha(r)\zeta(r)}}{2\alpha(r)}. \qquad (66)$$

Circular orbits correspond to extrema of $V_{\rm spin}(r)$, satisfying the condition $dV_{\rm spin}/dr = 0$, while their stability is determined by the sign of the second derivative: stable circular orbits require $d^2V_{\rm spin}/dr^2 > 0$, while $d^2V_{\rm spin}/dr^2 < 0$ indicates instability. The innermost stable circular orbit (ISCO) is located at the radius where $d^2V_{\rm spin}/dr^2 = 0$, marking the transition from stable to unstable circular motion.

The effective potential (66) encodes the combined influence of several distinct physical effects:

- *Spacetime curvature*: The metric function $f(r)$ determines the gravitational potential well and appears throughout $\alpha(r)$, $\delta(r)$, and $\zeta(r)$.
- *Quantum corrections*: The RNC $G(r) = G_0 r^2/(r^2 + \alpha G_0)$ modifies $f(r)$ and its derivatives $f'(r)$, producing quantum-induced softening of the gravitational interaction at small radii.
- *Spin-curvature coupling*: The spin parameter s enters through terms proportional to $f'(r)$ in p_t, p_ϕ, $\rho(r)$, $\delta(r)$, and $\zeta(r)$, coupling the particle's intrinsic angular momentum to the spacetime geometry.
- *Magnetic interaction*: The magnetic coupling parameter β appears in $\zeta(r)$ through the factor $(1-\beta\sqrt{f(r)})^2$, representing the energy shift due to magnetic dipole-field interactions.

For vanishing spin and magnetic moment ($s = \beta = 0$), the effective potential reduces to the standard geodesic potential for neutral test particles, $V_{\rm geo}(r) = \sqrt{f(r)(1 + J^2/r^2)}$, recovering the classical result.

E. Numerical analysis and physical interpretation

Figure 6 displays the effective potential $V_{\rm spin}(r)$ as a function of radial coordinate for various values of the spin parameter s and quantum parameter α. The background parameters are fixed to $M = 1.0$, $Q = 0.2$, and $G_0 = 1.0$, while the particle parameters are set to $m = 0.5$, $J = 0.3$, and $\beta = 0.05$. The curves correspond to spin values ranging from $s = 0$ (geodesic limit) to $s = 2.5$ in steps of $\Delta s = 0.5$, with line styles (solid, dashed, dotted) distinguishing different values of α.

An increase in the spin parameter s leads to a dramatic modification of the potential profile, particularly in the near-horizon region where relativistic effects and spin-curvature coupling are strongest. For fixed quantum parameters, higher spin values enhance the depth of the potential well by factors of 1.5-2.5 and shift the position of the potential minimum (corresponding to stable circular orbits) toward smaller radii. This inward migration occurs because larger spin amplifies

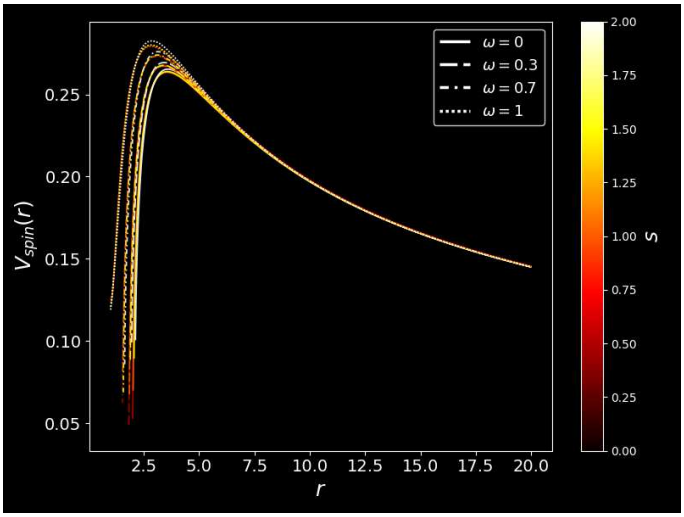


FIG. 6. Effective potential $V_{\rm spin}(r)$ governing the radial motion of a spinning magnetized test particle as a function of radial coordinate r. Curves correspond to different spin parameter values s increased in steps of $\Delta s = 0.5$. Line styles represent different quantum parameter values: solid ($\alpha = 0.0$, classical limit), dashed ($\alpha = 0.1$), dotted ($\alpha = 0.3$). Background parameters: $M = 1.0$, $Q = 0.2$, $G_0 = 1.0$. Particle parameters: $m = 0.5$, $J = 0.3$, $\beta = 0.05$. Higher spin deepens the potential well and shifts stable orbits inward, while larger quantum parameter softens the potential and displaces orbits outward.

the coupling term $sJf'(r)$ in the four-momentum components (58)-(59), which effectively increases the attractive gravitational interaction experienced by the spinning particle. The potential barrier height also increases with s, making it more difficult for particles to escape from bound orbits and enhancing the trapping efficiency of the BH.

Comparing curves with different line styles reveals the role of the quantum parameter α. For fixed spin s, increasing α from 0 (classical RN limit) to 0.3 leads to a noticeable softening of the effective potential, manifested by a reduction in the barrier height by 20-35% and a displacement of the stable circular orbit toward larger radii by $\Delta r \approx 0.3$-$0.5M$. This behavior can be traced to the suppression of the gravitational interaction induced by the running coupling $G(r)$, which reduces both the direct gravitational potential depth and the spin-curvature coupling terms proportional to $f'(r)$. The net effect is a weakening of the particle trapping mechanism, making it easier for particles to escape from the near-horizon region and raising the ISCO radius.

The interplay between spin and quantum corrections produces competing effects on the orbital structure. Spin tends to deepen the potential and draw stable orbits inward, while quantum corrections tend to soften the potential and push orbits outward. For moderate spin values $s \sim 1$-1.5 and moderate quantum parameters $\alpha \sim 0.1$-0.2, these effects partially cancel, resulting in orbital radii comparable to the classical geodesic case but with modified stability properties. For extreme parameter combinations (large s and large α simultaneously), the potential can develop multiple extrema corresponding to families of stable and unstable circular orbits at different radii, producing a richer orbital structure

than found in either classical RN or non-spinning quantum-corrected solutions.

The dependence of V_{spin} on the spin parameter is particularly pronounced for small radii $r \lesssim 3M$, where the spin-curvature coupling terms $\propto sf'(r)$ and $\propto s^2(f'(r))^2$ contribute significantly to the effective potential. In this regime, the running of the Newton constant modifies $f'(r)$ through both direct and derivative effects, amplifying the impact of quantum corrections on spinning particle dynamics. In contrast, at large distances $r \gg \max(M, \sqrt{\alpha G_0})$, all curves tend to merge regardless of s or α, reflecting the asymptotic recovery of flat-space particle dynamics and the diminishing influence of both spin and quantum effects.

VIII. CONCLUDING REMARKS

In this work, we investigated a QCCBH solution characterized by a position-dependent Newton constant $G(r) = G_0 r^2/(r^2 + \alpha G_0)$ derived from RG flow equations in asymptotically safe gravity. Our primary objective was to examine how the running of the gravitational coupling modifies the dynamical, thermodynamic, and mechanical properties of charged BH spacetimes, with particular attention to observable signatures that could distinguish quantum-corrected geometries from their classical RN counterparts.

We began by analyzing the metric structure and horizon properties of the quantum-corrected solution. The metric function $f(r) = 1 - 2G(r)M/r + Q^2/r^2$ exhibits qualitatively different behavior compared to classical RN geometry due to the suppression of the gravitational term at small radii. We found that the running coupling shifts the event horizon locations and modifies the extremality condition, with the critical charge parameter decreasing according to $Q_{\text{crit}} = \sqrt{G_0 M^2 - \alpha}$ as quantum corrections become stronger. These modifications are most pronounced for intermediate charge values $Q \sim 0.3$-$0.6M$ where the interplay between the quantum-corrected Schwarzschild term and the electromagnetic Coulomb term produces nontrivial competition in determining the horizon structure.

For fermionic perturbations, we derived the effective Schrdinger-like potential governing massless Dirac fields using the standard tetrad formalism and computed the QNM spectrum via the first-order WKB approximation. Table II presented the QNM frequencies for various combinations of the effective gravitational coupling G_0, quantum parameter α, angular quantum number κ, and overtone number n. We observed that reducing G_0 from 1.0 to 0.8 increased the real oscillation frequency $\text{Re}(\omega)$ by approximately 15-25% while simultaneously decreasing the imaginary damping rate $|\text{Im}(\omega)|$ by 20-35% for fundamental modes. Similarly, increasing the quantum parameter α from 0.1 to 0.3 enhanced $\text{Re}(\omega)$ by 2-5% and reduced $|\text{Im}(\omega)|$ by 25-40%, indicating that quantum corrections primarily affect the near-horizon structure of the effective potential where the modified metric function deviates most strongly from classical behavior.

The quality factor analysis in Table III quantified the relative persistence of oscillatory modes through the ratio $\mathcal{Q} = \text{Re}(\omega)/(2|\text{Im}(\omega)|)$. We found that $\mathcal{Q}$ decreased monotonically with overtone number n, following the approximate scaling $\mathcal{Q}_n \approx \mathcal{Q}_0/(2n+1)$ characteristic of single-barrier WKB spectra. For fixed overtone, quality factors increased with angular quantum number κ, reflecting enhanced mode trapping due to the centrifugal barrier in the effective Dirac potential given by Eq. (36). Comparing with classical RN values, we determined that quantum corrections at $G_0 = 0.8$ and $\alpha = 0.3$ raised $\mathcal{Q}$ by approximately 104% relative to the classical limit, indicating substantially longer-lived fermionic modes in the quantum-corrected geometry. This enhancement arises because the softening of the gravitational potential reduces barrier penetration probability, extending the characteristic decay timescale of trapped modes.

Our tidal force analysis through the geodesic deviation equation revealed qualitatively new features absent in classical charged BH spacetimes. We derived explicit expressions for the radial and angular tidal tensor components in Eq. (42), which depend on the first and second derivatives of the metric function $f(r)$. These derivatives inherit nontrivial structure from the running coupling $G(r)$, allowing both radial and angular tidal forces to change sign at specific radii determined by the quantum parameters. We calculated the radial transition radius r_{rad} from Eq. (48) and the angular transition radius r_{ang} from Eq. (50), finding that quantum corrections with $\alpha = 0.1$ shifted the angular inversion point outward by a factor of 5.5 compared to the classical RN value for $Q = 0.2$. This demonstrates that an infalling extended object would experience a progressive reorganization of its deformation pattern as it crosses these transition radii, undergoing stretching and compression direction reversals that have no analogue in standard general relativity.

For spinning magnetized particle dynamics, we employed the MPD formalism supplemented with the Tulczyjew spin supplementary condition to derive the effective potential $V_{\text{spin}}(r)$ governing radial motion. The potential in Eq. (66) incorporates contributions from spacetime curvature, spin-curvature coupling through terms proportional to $sf'(r)$, magnetic interaction energy via the factor $(1 - \beta\sqrt{f(r)})^2$, and quantum corrections through the RNC. Figure 6 illustrated how increasing the spin parameter s deepened the potential well and shifted stable circular orbit locations inward by $\Delta r \approx 0.3$-$0.5M$, while increasing the quantum parameter α produced a softening effect that displaced orbits outward by comparable amounts. These competing effects led to a rich orbital structure where moderate parameter values $s \sim 1$-1.5 and $\alpha \sim 0.1$-0.2 partially cancelled each other, yielding orbital radii close to the classical geodesic case but with modified stability properties. For extreme parameter combinations with both large s and large α, we found that the potential could develop multiple extrema corresponding to families of stable and unstable circular orbits at different radii, enriching the orbital structure beyond what appears in either classical RN or non-spinning quantum-corrected solutions.

Throughout our analysis, we verified that quantum corrections remained most significant in the near-horizon region $r \lesssim 3M$ where the running of the Newton constant pro-

duces measurable deviations from classical predictions, while asymptotically recovering standard RN behavior at large distances $r \gg \sqrt{\alpha G_0}$. This transition between quantum-dominated and classical regimes occurred smoothly without introducing singularities or pathological features in the metric, demonstrating that the asymptotically safe gravity framework provides a well-behaved regularization of the classical charged BH solution.

Looking forward, several natural extensions of this work merit investigation. First, the calculation of greybody factors and absorption cross sections for Dirac fields would provide additional probes of the quantum-corrected near-horizon structure and could reveal measurable deviations in Hawking radiation spectra that complement the temperature modifications already computed [146, 169–171]. Second, the analysis of electromagnetic QNMs and scalar perturbations would complete the perturbative stability picture and allow direct comparison with gravitational wave observations from hypothetical charged compact object mergers or superradiant instabilities in magnetized environments [172, 173]. Third, extending the tidal force analysis to include dynamical tides during inspiral phases would enable quantitative predictions for tidal heating rates and orbital decay timescales in extreme mass ratio inspirals observable by future space-based detectors such as LISA, potentially constraining the quantum parameter α through precision measurements of waveform phase evolution [174, 175].

On the astrophysical front, investigating photon sphere properties and gravitational lensing observables would connect our quantum-corrected solution to Event Horizon Telescope (EHT) shadow measurements and strong lensing observations, providing model-independent constraints on running coupling parameters through comparison with current and future imaging data. The spinning magnetized particle dynamics analysis could be extended to model accretion disk physics around charged compact objects, predicting modifications to the innermost stable circular orbit (ISCO) radius and characteristic emission radii that would alter X-ray continuum spectra in ways potentially detectable by missions such as XRISM or Athena. Additionally, exploring thermodynamic topology through analysis of critical points and phase transitions in the extended phase space would clarify the thermodynamic structure of QCCBHs and potentially reveal new scaling relations connecting quantum parameters to geometric phase transition properties.

Finally, generalizing the current framework to incorporate rotation through quantum-corrected Kerr-Newman-type solutions would enable investigation of spinning charged BHs with running couplings, which are arguably more astrophysically relevant than static configurations. Such solutions would provide fertile ground for studying the interplay between frame-dragging effects, electromagnetic interactions, and quantum gravitational corrections in realistic BH scenarios. The techniques developed here for analyzing Dirac perturbations, tidal forces, and spinning particle motion should extend naturally to rotating backgrounds, though the increased complexity of the metric structure would require more advanced numerical methods for computing QNM spectra and effective potentials.

ACKNOWLEDGMENTS

I.S. and E. S express their sincere appreciation to TÜBİTAK and ANKOS for their valuable assistance and continued support. İ.S. also acknowledges the essential support provided by COST Actions CA22113, CA21106, CA23130, and CA23115, which play a crucial role in facilitating international collaboration and strengthening networking opportunities within the scientific community.

[1] H. Reissner, "Über die Eigengravitation des elektrischen Feldes nach der Einsteinschen Theorie," Annalen Phys. **355**, 106–120 (1916).
[2] Gunnar Nordström, "On the energy of the gravitation field in einsteins theory," Koninklijke Nederlandse Akademie van Wetenschappen Proceedings Series B Physical Sciences **20**, 1238–1245 (1918).
[3] Hans Stephani, Dietrich Kramer, Malcolm MacCallum, Cornelius Hoenselaers, and Eduard Herlt, *Exact solutions of Einstein's field equations* (Cambridge university press, 2009).
[4] Erdem Sucu and İzzet Sakall, "Exploring Lorentz-violating effects of Kalb-Ramond field on charged black hole thermodynamics and photon dynamics," Phys. Rev. D **111**, 064049 (2025).
[5] Stephen William Hawking and Roger Penrose, "The singularities of gravitational collapse and cosmology," Proceedings of the Royal Society of London. A. Mathematical and Physical Sciences **314**, 529–548 (1970).
[6] John Preskill, "Do black holes destroy information," in *Proceedings of the International Symposium on Black Holes, Membranes, Wormholes and Superstrings, S. Kalara and DV Nanopoulos, eds.(World Scientific, Singapore, 1993) pp* (World Scientific, 1992) pp. 22–39.
[7] Eloy Ayon-Beato and Alberto Garcia, "Regular black hole in general relativity coupled to nonlinear electrodynamics," Physical review letters **80**, 5056 (1998).
[8] Oliver Lauscher and Martin Reuter, "Ultraviolet fixed point and generalized flow equation of quantum gravity," Physical Review D **65**, 025013 (2001).
[9] João Lucas Miqueleto and André G. S. Landulfo, "Exact renormalization group, entanglement entropy, and black hole entropy," Phys. Rev. D **103**, 045012 (2021), arXiv:2008.04951 [gr-qc].
[10] Martin Reuter, "Nonperturbative evolution equation for quantum gravity," Physical Review D **57**, 971 (1998).
[11] Max Niedermaier, "The asymptotic safety scenario in quantum gravity: an introduction," Classical and Quantum Gravity **24**, R171 (2007).
[12] Steven Weinberg, "Ultraviolet Divergences in Cosmo-

logical Correlations," Phys. Rev. D **83**, 063508 (2011), arXiv:1011.1630 [hep-th].
[13] Martin Reuter and Frank Saueressig, "Renormalization group flow of quantum gravity in the einstein-hilbert truncation," Physical Review D **65**, 065016 (2002).
[14] Daniel F Litim, "Renormalization group and the planck scale," Philosophical Transactions of the Royal Society A: Mathematical, Physical and Engineering Sciences **369**, 2759–2778 (2011).
[15] Daniel F Litim, "Fixed points of quantum gravity," Physical review letters **92**, 201301 (2004).
[16] Alfio Bonanno and Martin Reuter, "Renormalization group improved black hole space-times," Phys. Rev. D **62**, 043008 (2000), arXiv:hep-th/0002196.
[17] A Bukhari, G Abbas, and Tao Zhu, "Orbital structure and radiative behavior of accretion disks around quantum-corrected charged black holes," Journal of High Energy Astrophysics , 100550 (2026).
[18] Kevin Falls, Daniel F. Litim, and Aarti Raghuraman, "Black Holes and Asymptotically Safe Gravity," Int. J. Mod. Phys. A **27**, 1250019 (2012), arXiv:1002.0260 [hep-th].
[19] Abdel Nasser Tawfik and Abdel Magied Diab, "A review of the generalized uncertainty principle," Reports on Progress in Physics **78**, 126001 (2015).
[20] Ganim Gecim and Yusuf Sucu, "Quantum gravity correction to hawking radiation of the 2+ 1-dimensional wormhole," Advances in High Energy Physics **2020**, 7516789 (2020).
[21] Pasquale Bosso, Giuseppe Gaetano Luciano, Luciano Petruzziello, and Fabian Wagner, "30 years in: Quo vadis generalized uncertainty principle?" Classical and Quantum Gravity **40**, 195014 (2023).
[22] İzzet Sakallı, Yusuf Sucu, and Erdem Sucu, "Zitterbewegung oscillations and GUP-induced quantum modifications of Yang-Mills black holes in perfect fluid dark matter," Nucl. Phys. B **1022**, 117216 (2026).
[23] Michele Maggiore, "A generalized uncertainty principle in quantum gravity," Physics Letters B **304**, 65–69 (1993).
[24] Ganim Gecim and Yusuf Sucu, "Quantum gravity effect on the hawking radiation of spinning dilaton black hole," The European Physical Journal C **79**, 882 (2019).
[25] Erdem Sucu and Izzet Sakalli, "Ads black holes in einstein-kalb-ramond gravity: Quantum corrections, phase transitions, and orbital dynamics," NUCLEAR PHYSICS B **1018** (2025), 10.1016/j.nuclphysb.2025.117081.
[26] Roberto Casadio and Fabio Scardigli, "Generalized uncertainty principle, classical mechanics, and general relativity," Physics Letters B **807**, 135558 (2020).
[27] CAVİT Tekincay, Ganim Gecim, and YUSUF Sucu, "Zitterbewegung particles tunneling from reissner-nordström ads black hole surrounded by quintessence," Europhysics Letters **135**, 31003 (2021).
[28] Erdem Sucu and İzzet Sakallı, "Scalar-tensor corrections and observational signatures of hairy black holes in Horndeski gravity," High Energy Dens. Phys. **56**, 101220 (2025).
[29] Ahmed Farag Ali, Saurya Das, and Elias C Vagenas, "Discreteness of space from the generalized uncertainty principle," Physics Letters B **678**, 497–499 (2009).
[30] Erdem Sucu, "Quantum gravity corrections and plasma-induced lensing of magnetically charged black holes," Nucl. Phys. B **1022**, 117285 (2026).
[31] Salvatore Capozziello, Gaetano Lambiase, and Gaetano Scarpetta, "Generalized uncertainty principle from quantum geometry," arXiv preprint gr-qc/9910017 (1999).
[32] Erdem Sucu and İzzet Sakallı, "Charged regular black holes in quantum gravity: from thermodynamic stability to observational phenomena," The European Physical Journal C **85**, 989 (2025).
[33] Cavit Tekincay, Mustafa Dernek, and Yusuf Sucu, "Exotic criticality of the btz black hole," The European Physical Journal Plus **136**, 222 (2021).
[34] Faizuddin Ahmed, Ahmad Al-Badawi, İzzet Sakallı, and Abdelmalek Bouzenadad, "Quasinormal modes and GUP-corrected Hawking radiation of BTZ black holes within modified gravity frameworks," Nucl. Phys. B **1011**, 116806 (2025), arXiv:2412.04513 [gr-qc].
[35] Sara Kanzi and İzzet Sakallı, "GUP-modified Hawking radiation and transmission/reflection coefficients of rotating polytropic black hole," Eur. Phys. J. Plus **137**, 14 (2022), arXiv:2107.11776 [hep-th].
[36] Behnam Pourhassan, Ali Övgün, and İzzet Sakallı, "PV criticality of Achucarro-Ortiz black hole in the presence of higher order quantum and GUP corrections," Int. J. Geom. Meth. Mod. Phys. **17**, 2050156 (2020), arXiv:1811.02193 [gr-qc].
[37] Faizuddin Ahmed, İzzet Sakallı, Ahmad Al-Badawi, and Abdelmalek Bouzenada, "Perturbations and modified hawking radiation in cylindrical black holes within f(R) and Ricci-Inverse gravity theories," Int. J. Mod. Phys. A **40**, 2550171 (2025), arXiv:2501.00060 [gr-qc].
[38] İzzet Sakallı and Sara Kanzi, "Physical properties of brane-world black hole solutions via a confining potential," Annals Phys. **439**, 168803 (2022), arXiv:2201.00537 [hep-th].
[39] Kenichi Konishi, Giampiero Paffuti, and Paolo Provero, "Minimum physical length and the generalized uncertainty principle in string theory," Physics Letters B **234**, 276–284 (1990).
[40] Erdem Sucu and İzzet Sakallı, "Quantum-corrected thermodynamics and plasma lensing of mog black holes," Proceedings of the Royal Society A: Mathematical, Physical and Engineering Sciences **481** (2025).
[41] Carlo Rovelli, "Loop quantum gravity," Living reviews in relativity **11**, 5 (2008).
[42] Giuseppe Gaetano Luciano and Luciano Petruzziello, "Generalized uncertainty principle and its implications on geometric phases in quantum mechanics," The European Physical Journal Plus **136**, 179 (2021).
[43] Abhay Ashtekar and Parampreet Singh, "Loop quantum cosmology: a status report," Classical and Quantum Gravity **28**, 213001 (2011).
[44] Fabio Scardigli, "Generalized uncertainty principle in quantum gravity from micro-black hole gedanken experiment," Physics Letters B **452**, 39–44 (1999).
[45] Yun Soo Myung, Yong-Wan Kim, and Young-Jai Park, "Black hole thermodynamics with generalized uncertainty principle," Physics Letters B **645**, 393–397 (2007).
[46] Saurya Das and Elias C Vagenas, "Universality of quantum gravity corrections," Physical review letters **101**, 221301 (2008).
[47] Kourosh Nozari and Sara Saghafi, "Natural cutoffs and quantum tunneling from black hole horizon," Journal of High Energy Physics **2012**, 1–18 (2012).
[48] E Sucu and İ Sakallı, "Gup-reinforced hawking radiation in rotating linear dilaton black hole spacetime," Physica Scripta **98**, 105201 (2023).
[49] Adam D Helfer, "Hawking radiation, quantum fields, and tunneling," Physical Review D **100**, 025005 (2019).

[50] Erdem Sucu and İzzet Sakallı, "Astrophysical reality of black hole thermodynamics and dynamics: Transformative influence of Hernquist dark matter distributions," Phys. Dark Univ. **49**, 102051 (2025).

[51] Mark Ho-Yeuk Cheung, Digvijay Wadekar, Ajit Kumar Mehta, Tousif Islam, Javier Roulet, Emanuele Berti, Tejaswi Venumadhav, Barak Zackay, and Matias Zaldarriaga, "Searching for intermediate mass ratio binary black hole mergers in the third observing run of LIGO-Virgo-KAGRA," Phys. Rev. D **113**, 023003 (2026), arXiv:2507.01083 [gr-qc].

[52] Benjamin P Abbott, Richard Abbott, Thomas D Abbott, Matthew R Abernathy, Fausto Acernese, Kendall Ackley, Carl Adams, Thomas Adams, Paolo Addesso, Rana X Adhikari, *et al.*, "Observation of gravitational waves from a binary black hole merger," Physical review letters **116**, 061102 (2016).

[53] Martti Raidal, Ville Vaskonen, and Hardi Veermäe, "Gravitational waves from primordial black hole mergers," Journal of Cosmology and Astroparticle Physics **2017**, 037 (2017).

[54] BP Abbott, R Abbott, TD Abbott, S Abraham, Fausto Acernese, K Ackley, C Adams, Rana X Adhikari, VB Adya, C Affeldt, *et al.*, "Tests of general relativity with the binary black hole signals from the ligo-virgo catalog gwtc-1," Physical Review D **100**, 104036 (2019).

[55] Olaf Dreyer, Bernard Kelly, Badri Krishnan, Lee Samuel Finn, David Garrison, and Ramon Lopez-Aleman, "Black-hole spectroscopy: testing general relativity through gravitational-wave observations," Classical and Quantum Gravity **21**, 787 (2004).

[56] Kazunori Akiyama *et al.* (Event Horizon Telescope), "First Sagittarius A* Event Horizon Telescope Results. I. The Shadow of the Supermassive Black Hole in the Center of the Milky Way," Astrophys. J. Lett. **930**, L12 (2022), arXiv:2311.08680 [astro-ph.HE].

[57] Kazunori Akiyama *et al.* (Event Horizon Telescope), "First Sagittarius A* Event Horizon Telescope Results. VI. Testing the Black Hole Metric," Astrophys. J. Lett. **930**, L17 (2022), arXiv:2311.09484 [astro-ph.HE].

[58] Kazunori Akiyama *et al.* (Event Horizon Telescope), "First M87 Event Horizon Telescope Results. I. The Shadow of the Supermassive Black Hole," Astrophys. J. Lett. **875**, L1 (2019), arXiv:1906.11238 [astro-ph.GA].

[59] Kazunori Akiyama *et al.* (Event Horizon Telescope), "First M87 Event Horizon Telescope Results. IV. Imaging the Central Supermassive Black Hole," Astrophys. J. Lett. **875**, L4 (2019), arXiv:1906.11241 [astro-ph.GA].

[60] Dimitrios Psaltis, "Testing General Relativity with the Event Horizon Telescope," Gen. Rel. Grav. **51**, 137 (2019), arXiv:1806.09740 [astro-ph.HE].

[61] RA Konoplya, "Quasinormal modes and grey-body factors of regular black holes with a scalar hair from the effective field theory," Journal of Cosmology and Astroparticle Physics **2023**, 001 (2023).

[62] Emanuele Berti, Vitor Cardoso, and Andrei O Starinets, "Quasinormal modes of black holes and black branes," Classical and Quantum Gravity **26**, 163001 (2009).

[63] ALFREDO López-Ortega, "Quasinormal frequencies of the dirac field in the massless topological black hole," Revista mexicana de física **56**, 44–53 (2010).

[64] Angel Rincon, Sharmanthie Fernando, Grigoris Panotopoulos, and Leonardo Balart, "Quasinormal modes and absorption cross-section of a bardeen black hole surrounded by perfect fluid dark matter in four dimensions," arXiv preprint arXiv:2504.05215 (2025).

[65] RA Konoplya, "Quantum corrected black holes: Quasinormal modes, scattering, shadows," Physics Letters B **804**, 135363 (2020).

[66] İzzet Sakalli and Sara Kanzi, "Topical Review: greybody factors and quasinormal modes for black holes in various theories - fingerprints of invisibles," Turk. J. Phys. **46**, 51–103 (2022), arXiv:2205.01771 [hep-th].

[67] Ahmad Al-Badawi, Sara Kanzi, and İzzet Sakallı, "Fermionic and bosonic greybody factors as well as quasinormal modes for charged Taub NUT black holes," Annals Phys. **452**, 169294 (2023), arXiv:2203.04140 [hep-th].

[68] İzzet Sakalli and Gülnihal Tokgöz Hyusein, "Quasinormal modes of charged fermions in linear dilaton black hole spacetime:exact frequencies," Turk. J. Phys. **45**, 43–58 (2021), arXiv:2102.03595 [hep-th].

[69] Sara Kanzi and İzzet Sakallı, "Greybody radiation and quasinormal modes of Kerr-like black hole in Bumblebee gravity model," Eur. Phys. J. C **81**, 501 (2021), arXiv:2102.06303 [hep-th].

[70] Akhil Uniyal, Sara Kanzi, and İzzet Sakallı, "Some observable physical properties of the higher dimensional dS/AdS black holes in Einstein-bumblebee gravity theory," Eur. Phys. J. C **83**, 668 (2023), arXiv:2207.10122 [hep-th].

[71] İzzet Sakallı, Erdem Sucu, Ahmad Al-Badawi, and Faizuddin Ahmed, "Optical appearance, Hawking radiation, and Barrow thermodynamics of Letelier black hole in electromagnetic universe," (2025), arXiv:2512.18881 [gr-qc].

[72] I. Sakalli and G. Tokgoz, "Resonance Spectra of Caged Stringy Black Hole and Its Spectroscopy," Adv. High Energy Phys. **2015**, 739153 (2015), arXiv:1502.02274 [gr-qc].

[73] Hing Tong Cho, "Dirac quasinormal modes in schwarzschild black hole spacetimes," Physical Review D **68**, 024003 (2003).

[74] Semra Gurtas Dogan and Yusuf Sucu, "Quasinormal modes of dirac field in 2+ 1 dimensional gravitational wave background," Physics Letters B **797**, 134839 (2019).

[75] Ji-liang Jing, "Dirac quasinormal modes of the Reissner-Nordstrom de Sitter black hole," Phys. Rev. D **69**, 084009 (2004), arXiv:gr-qc/0312079.

[76] Kostas D Kokkotas and Bernd G Schmidt, "Quasi-normal modes of stars and black holes," Living Reviews in Relativity **2**, 2 (1999).

[77] Mengjie Wang, Carlos Herdeiro, and Jiliang Jing, "Charged Dirac perturbations on Reissner-Nordström–anti–de Sitter spacetimes: Quasinormal modes with Robin boundary conditions," Phys. Rev. D **100**, 124062 (2019), arXiv:1910.14305 [gr-qc].

[78] Roman A Konoplya and Alexander Zhidenko, "Quasinormal modes of massive fermions in kerr spacetime: Long-lived modes and the fine structure," Physical Review D **97**, 084034 (2018).

[79] Mauricio Richartz, "Quasinormal modes of extremal black holes," Physical Review D **93**, 064062 (2016).

[80] Hao-Tse Huang and Wenbin Lu, "Tidal disruption rate suppression by the event horizon of spinning black holes," Mon. Not. Roy. Astron. Soc. **527**, 1865–1883 (2023), arXiv:2301.00259 [astro-ph.GA].

[81] Michela Silvestrini, Elisa Maggio, Sumanta Chakraborty, and Paolo Pani, "Tidal deformations of compact objects from the membrane paradigm," Phys. Rev. D **112**, 124021 (2025), arXiv:2506.16516 [gr-qc].

[82] Haroldo CD Lima and Luís CB Crispino, "Tidal forces in

the charged hayward black hole spacetime," International Journal of Modern Physics D **29**, 2041014 (2020).
[83] Luís C. B. Crispino, Atsushi Higuchi, Leandro A. Oliveira, and Ednilton S. de Oliveira, "Tidal forces in Reissner–Nordström spacetimes," Eur. Phys. J. C **76**, 168 (2016), arXiv:1602.07232 [gr-qc].
[84] Daniela S. J. Cordeiro, Ednaldo L. B. Junior, José Tarciso S. S. Junior, Francisco S. N. Lobo, Manuel E. Rodrigues, Diego Rubiera-Garcia, Luís F. Dias da Silva, and Henrique A. Vieira, "Free-falling test particles in a charged Kalb-Ramond black hole: Gravitational Doppler effect and tidal forces," Phys. Rev. D **112**, 104018 (2025), arXiv:2503.12048 [gr-qc].
[85] Ming Zhang and Jie Jiang, "Stable circular orbits of spinning test particles around accelerating Kerr black hole," Phys. Rev. D **101**, 104012 (2020), arXiv:2004.13016 [gr-qc].
[86] Donato Bini, Fernando de Felice, and Andrea Geralico, "Spinning test particles and clock effect in schwarzschild spacetime," Classical and Quantum Gravity **21**, 5427 (2004).
[87] Michael D Hartl, "Dynamics of spinning test particles in kerr spacetime," Physical Review D **67**, 024005 (2003).
[88] L. Filipe O. Costa, José Natário, and Miguel Zilhao, "Spacetime dynamics of spinning particles: Exact electromagnetic analogies," Phys. Rev. D **93**, 104006 (2016), arXiv:1207.0470 [gr-qc].
[89] Giovanni Modanese, "Effect of a scale-dependent cosmological term on the motion of small test particles in a schwarzschild background," Nuclear Physics B **556**, 397–408 (1999).
[90] Jacob D Bekenstein, "Black holes and entropy," Physical Review D **7**, 2333 (1973).
[91] Stephen W Hawking, "Particle creation by black holes," Communications in mathematical physics **43**, 199–220 (1975).
[92] Nicholas David Birrell and Paul Charles William Davies, *Quantum fields in curved space* (Cambridge university press, 1984).
[93] Maria Alberti and Jochen Zahn, "Quantum effects in near-extremal charged black hole spacetimes," Phys. Rev. D **111**, 104061 (2025), arXiv:2501.05549 [gr-qc].
[94] Nusret Sahan, Erdem Sucu, and Yusuf Sucu, "Quantum phase transitions of dirac particles in a magnetized rotating curved background: Interplay of geometry, magnetization, and thermodynamics," Physics of the Dark Universe , 102005 (2025).
[95] Sabine Hossenfelder, "Minimal length scale scenarios for quantum gravity," Living Reviews in Relativity **16**, 2 (2013).
[96] Ahmed Farag Ali, Saurya Das, and Elias C Vagenas, "The generalized uncertainty principle and quantum gravity phenomenology," in *The Twelfth Marcel Grossmann Meeting: On Recent Developments in Theoretical and Experimental General Relativity, Astrophysics and Relativistic Field Theories (In 3 Volumes)* (World Scientific, 2012) pp. 2407–2409.
[97] Kartik Joshi, Sanjib Dey, and Satyajit Jena, "Probing Planck scale effects on absolute mass limit in neutrino flavor evolution," Nucl. Phys. B **1019**, 117118 (2025), arXiv:2506.07588 [hep-ph].
[98] Ekrem Aydiner, Erdem Sucu, and İzzet Sakallı, "Regular magnetically charged black holes from nonlinear electrodynamics: Thermodynamics, light deflection, and orbital dynamics," Phys. Dark Univ. **50**, 102164 (2025), arXiv:2507.05145 [gr-qc].
[99] H. Ramezani and K. Nozari, "Linear–quadratic GUP and thermodynamic dimensional reduction," Annals Phys. **469**, 169752 (2024), arXiv:2407.20497 [gr-qc].
[100] Pasquale Bosso and Juan Manuel López Vega, "Minimal length phenomenology and the black body radiation," Class. Quant. Grav. **39**, 175001 (2022), arXiv:2112.04609 [gr-qc].
[101] Ganim Gecim and Yusuf Sucu, "Quantum gravity effect on the tunneling particles from warped-ads3 black hole," Modern Physics Letters A **33**, 1850164 (2018).
[102] Achim Kempf, Gianpiero Mangano, and Robert B. Mann, "Hilbert space representation of the minimal length uncertainty relation," Phys. Rev. D **52**, 1108–1118 (1995), arXiv:hep-th/9412167.
[103] Achim Kempf and Gianpiero Mangano, "Minimal length uncertainty relation and ultraviolet regularization," Phys. Rev. D **55**, 7909–7920 (1997), arXiv:hep-th/9612084.
[104] F. Brau, "Minimal length uncertainty relation and hydrogen atom," J. Phys. A **32**, 7691–7696 (1999), arXiv:quant-ph/9905033.
[105] Kourosh Nozari and S Hamid Mehdipour, "Parikh-wilczek tunneling from noncommutative higher dimensional black holes," Journal of High Energy Physics **2009**, 061 (2009).
[106] G Gecim and Y Sucu, "Dirac and scalar particles tunnelling from topological massive warped-ads3 black hole," Astrophysics and Space Science **357**, 105 (2015).
[107] Ganim Gecim and Yusuf Sucu, "The gup effect on hawking radiation of the 2+ 1 dimensional black hole," Physics Letters B **773**, 391–394 (2017).
[108] Ganim Gecim and Yusuf Sucu, "Quantum gravity effect on the tunneling particles from 2+ 1-dimensional new-type black hole," Advances in High Energy Physics **2018**, 8728564 (2018).
[109] Zhen-Yu Liu and Ji-Rong Ren, "Fermions tunnelling with quantum gravity correction," Commun. Theor. Phys. **62**, 819–823 (2014), arXiv:1403.7307 [gr-qc].
[110] Özlem Yeşiltaş, "Dirac equation in the curved spacetime and generalized uncertainty principle: A fundamental quantum mechanical approach with energy-dependent potentials," The European Physical Journal Plus **134**, 331 (2019).
[111] Deyou Chen, Houwen Wu, and Haitang Yang, "Fermion's tunnelling with effects of quantum gravity," Adv. High Energy Phys. **2013**, 432412 (2013), arXiv:1305.7104 [gr-qc].
[112] Maulik K Parikh and Frank Wilczek, "Hawking radiation as tunneling," Physical review letters **85**, 5042 (2000).
[113] Ryan Kerner and Robert B. Mann, "Fermions tunnelling from black holes," Class. Quant. Grav. **25**, 095014 (2008), arXiv:0710.0612 [hep-th].
[114] K Srinivasan and T Padmanabhan, "Particle production and complex path analysis," Physical Review D **60**, 024007 (1999).
[115] Petr Hajicek, "Origin of hawking radiation," Physical Review D **36**, 1065 (1987).
[116] Roberto Casadio, Piero Nicolini, and Roldão Da Rocha, "Generalised uncertainty principle hawking fermions from minimally geometric deformed black holes," Classical and Quantum Gravity **35**, 185001 (2018).
[117] Ganim Gecim and Yusuf Sucu, "Quantum gravity effect on the Hawking radiation of charged rotating BTZ black hole," Gen. Rel. Grav. **50**, 152 (2018), arXiv:1804.10551 [gr-qc].
[118] Hare Krishna and Biswajit Sahoo, "Universality of loop corrected soft theorems in 4d," JHEP **11**, 233 (2023),

arXiv:2308.16807 [hep-th].
[119] Sean P. Robinson and Frank Wilczek, "A Relationship between Hawking radiation and gravitational anomalies," Phys. Rev. Lett. **95**, 011303 (2005), arXiv:gr-qc/0502074.
[120] Ryan Kerner and Robert B. Mann, "Tunnelling, temperature and Taub-NUT black holes," Phys. Rev. D **73**, 104010 (2006), arXiv:gr-qc/0603019.
[121] Pisin Chen and Ronald J Adler, "Black hole remnants and dark matter," Nuclear Physics B-Proceedings Supplements **124**, 103–106 (2003).
[122] Stephen W Hawking and Don N Page, "Thermodynamics of black holes in anti-de sitter space," Communications in Mathematical Physics **87**, 577–588 (1983).
[123] Marco M. Caldarelli, Guido Cognola, and Dietmar Klemm, "Thermodynamics of Kerr-Newman-AdS black holes and conformal field theories," Class. Quant. Grav. **17**, 399–420 (2000), arXiv:hep-th/9908022.
[124] David Kastor, Sourya Ray, and Jennie Traschen, "Enthalpy and the Mechanics of AdS Black Holes," Class. Quant. Grav. **26**, 195011 (2009), arXiv:0904.2765 [hep-th].
[125] Arun Kumar, Ashima Sood, J. K. Singh, Aroonkumar Beesham, and Sushant G. Ghosh, "Phase structure and critical behaviour of charged-AdS black holes with perfect fluid dark matter," Phys. Dark Univ. **40**, 101220 (2023).
[126] Natacha Altamirano, David Kubiznak, and Robert B. Mann, "Reentrant phase transitions in rotating anti–de Sitter black holes," Phys. Rev. D **88**, 101502 (2013), arXiv:1306.5756 [hep-th].
[127] John D Barrow, "The area of a rough black hole," Physics Letters B **808**, 135643 (2020).
[128] Jacob D Bekenstein, "Bekenstein-hawking entropy," Scholarpedia **3**, 7375 (2008).
[129] Saurya Das, Parthasarathi Majumdar, and Rajat K Bhaduri, "General logarithmic corrections to black-hole entropy," Classical and Quantum Gravity **19**, 2355 (2002).
[130] Rong-Gen Cai and Sang Pyo Kim, "First law of thermodynamics and friedmann equations offriedmann-robertson-walker universe," Journal of High Energy Physics **2005**, 050 (2005).
[131] Herbert B Callen, "Thermodynamics and an introduction to thermostatistics," John Wiley& Sons **2** (1993).
[132] Natacha Altamirano, David Kubiznak, and Robert B Mann, "Reentrant phase transitions in rotating ads black holes," arXiv preprint arXiv:1306.5756 (2013).
[133] Andrew Chamblin, Roberto Emparan, Clifford V. Johnson, and Robert C. Myers, "Charged AdS black holes and catastrophic holography," Phys. Rev. D **60**, 064018 (1999), arXiv:hep-th/9902170.
[134] Ran Li and Jin Wang, "Hawking radiation and Pv criticality of charged dynamical (Vaidya) black hole in anti-de Sitter space," Phys. Lett. B **813**, 136035 (2021), arXiv:2009.09319 [gr-qc].
[135] Brian P Dolan, "Pressure and volume in the first law of black hole thermodynamics," Classical and Quantum Gravity **28**, 235017 (2011).
[136] Natacha Altamirano, David Kubiznak, Robert B. Mann, and Zeinab Sherkatghanad, "Thermodynamics of rotating black holes and black rings: phase transitions and thermodynamic volume," Galaxies **2**, 89–159 (2014), arXiv:1401.2586 [hep-th].
[137] David Kubizňák, Robert B Mann, and Mae Teo, "Black hole chemistry: thermodynamics with lambda," Classical and Quantum Gravity **34**, 063001 (2017).
[138] D. Lynden-Bell, "Negative specific heat in astronomy, physics and chemistry," Physica A **263**, 293–304 (1999), arXiv:cond-mat/9812172.
[139] Guangzhou Guo, Peng Wang, Houwen Wu, and Haitang Yang, "Thermodynamics and phase structure of an einstein-maxwell-scalar model in extended phase space," Physical Review D **105**, 064069 (2022).
[140] Erdem Sucu, Izzet Sakallı, Özcan Sert, and Yusuf Sucu, "Quantum-corrected thermodynamics and plasma lensing in non-minimally coupled symmetric teleparallel black holes," Physics of the Dark Universe , 102063 (2025).
[141] Paul CW Davies, "Thermodynamic phase transitions of kerr-newman black holes in de sitter space," Classical and Quantum Gravity **6**, 1909 (1989).
[142] E. W. Leaver, "An Analytic representation for the quasi normal modes of Kerr black holes," Proc. Roy. Soc. Lond. A **402**, 285–298 (1985).
[143] Alfio Bonanno and Martin Reuter, "Renormalization group improved black hole spacetimes," Physical Review D **62**, 043008 (2000).
[144] Alfio Bonanno and Martin Reuter, "Spacetime structure of an evaporating black hole in quantum gravity," Physical Review DParticles, Fields, Gravitation, and Cosmology **73**, 083005 (2006).
[145] Bernard F Schutz and Clifford M Will, "Black hole normal modes: a semianalytic approach," The Astrophysical Journal **291**, L33–L36 (1985).
[146] Sai Iyer and Clifford M Will, "Black-hole normal modes: A wkb approach. i. foundations and application of a higher-order wkb analysis of potential-barrier scattering," Physical Review D **35**, 3621 (1987).
[147] Yusuf Sucu and Nuri Ünal, "Exact solution of dirac equation in 2+ 1 dimensional gravity," Journal of mathematical physics **48** (2007).
[148] Zlatko K. Minev, Khadijeh Najafi, Swarnadeep Majumder, Juven Wang, Ady Stern, Eun-Ah Kim, Chao-Ming Jian, and Guanyu Zhu, "Realizing string-net condensation: Fibonacci anyon braiding for universal gates and sampling chromatic polynomials," Nature Commun. **16**, 6225 (2025), arXiv:2406.12820 [quant-ph].
[149] Tong-Zheng Wang, Wei-Liang Qian, Juan Fernando Zapata Zapata, and Kai Lin, "Scalar and Dirac quasinormal modes of scalar-tensor-Gauss-Bonnet black holes," Chin. Phys. C **46**, 045101 (2022).
[150] Lev Davidovich Landau, Evgenii Mikhailovich Lifshitz, and Evgeniĭ Mikhaĭlovich Lifshits, *The Classical Theory of Fields: Volume 2*, Vol. 2 (Butterworth-Heinemann, 1975).
[151] Ignazio Ciufolini, "Dragging of inertial frames," Nature **449**, 41–47 (2007).
[152] Pritam Banerjee, Debojyoti Garain, Suvankar Paul, Rajibul Shaikh, and Tapobrata Sarkar, "Constraining modified gravity from tidal phenomena in binary stars," The Astrophysical Journal **910**, 23 (2021).
[153] Xing Zhang, Wen Zhao, He Huang, and Yifu Cai, "Post-newtonian parameters and cosmological constant of screened modified gravity," Physical Review D **93**, 124003 (2016).
[154] Daniela SJ Cordeiro, Ednaldo LB Junior, José Tarciso SS Junior, Francisco SN Lobo, Manuel E Rodrigues, Diego Rubiera-Garcia, Luís F Dias da Silva, and Henrique A Vieira, "Free-falling test particles in a charged kalb-ramond black hole: Gravitational doppler effect and tidal forces," Physical Review D **112**, 104018 (2025).
[155] Marek A. Abramowicz and P. Chris Fragile, "Foundations

of Black Hole Accretion Disk Theory," Living Rev. Rel. **16**, 1 (2013), arXiv:1104.5499 [astro-ph.HE].
[156] Bernard Carr and Florian Kühnel, "Primordial black holes as dark matter: recent developments," Annual Review of Nuclear and Particle Science **70**, 355–394 (2020).
[157] Nicholas C Stone, Brian D Metzger, and Zoltán Haiman, "Assisted inspirals of stellar mass black holes embedded in agn discs: solving the final au problem," Monthly Notices of the Royal Astronomical Society **464**, 946–954 (2017).
[158] Pau Amaro-Seoane, Heather Audley, Stanislav Babak, John Baker, Enrico Barausse, Peter Bender, Emanuele Berti, Pierre Binetruy, Michael Born, Daniele Bortoluzzi, *et al.*, "Laser interferometer space antenna," arXiv preprint arXiv:1702.00786 (2017).
[159] Thibault Damour and Alessandro Nagar, "Effective One Body description of tidal effects in inspiralling compact binaries," Phys. Rev. D **81**, 084016 (2010), arXiv:0911.5041 [gr-qc].
[160] Shokhzod Jumaniyozov, Javlon Rayimbaev, Munisbek Akhmedov, Yunus Turaev, Sulton Usanov, and Satimbay Palvanov, "Dynamics of charged-spinning particles around charged Kalb–Ramond black holes," Phys. Dark Univ. **50**, 102161 (2025).
[161] Erdem Sucu and İzzet Sakallı, "Dynamics of particles surrounding a stationary, spherically-symmetric black hole with Nonlinear Electrodynamics," Phys. Dark Univ. **47**, 101771 (2025).
[162] W. G. Dixon, "Dynamics of extended bodies in general relativity. II. Moments of the charge-current vector," Proc. Roy. Soc. Lond. A **319**, 509–547 (1970).
[163] G. d'Ambrosi, S. Satish Kumar, J. van de Vis, and J. W. van Holten, "Spinning bodies in curved spacetime," Phys. Rev. D **93**, 044051 (2016), arXiv:1511.05454 [gr-qc].
[164] M. I. Wanas and Mona M. Kamal, "Motion of Charged Spinning Particles in a Unified Field," Adv. High Energy Phys. **2021**, 4970469 (2021), arXiv:2110.05592 [hep-th].
[165] M. Leclerc, "Mathisson-Papapetrou equations in metric and gauge theories of gravity in a Lagrangian formulation," Class. Quant. Grav. **22**, 3203–3222 (2005), arXiv:gr-qc/0505021.
[166] W Tulczyjew, "Motion of multipole particles in general relativity theory," Acta Phys. Pol **18**, 94 (1959).
[167] Nuri Ünal, "Electromagnetic and gravitational interactions of the spinning particle," Journal of mathematical physics **47** (2006).
[168] Dilmurod Umarov, Farruh Atamurotov, Sushant G. Ghosh, Ahmadjon Abdujabbarov, and G. Mustafa, "Dynamics of spinning particles around static black holes in effective quantum gravity," Eur. Phys. J. C **85**, 800 (2025).
[169] Qian Li, Chen Ma, Yu Zhang, Zhi-Wen Lin, and Peng-Fei Duan, "Gray-body factor and absorption of the dirac field in estgb gravity," Chinese Journal of Physics **77**, 1269–1277 (2022).
[170] Mirjam Cvetič and Finn Larsen, "Greybody factors for black holes in four dimensions: Particles with spin," Physical Review D **57**, 6297 (1998).
[171] Zainab Malik, "Grey-Body Factors for Scalar and Dirac Fields in the Euler-Heisenberg Electrodynamics," Int. J. Grav. Theor. Phys. **1**, 6 (2025), arXiv:2509.15995 [gr-qc].
[172] Roman A Konoplya and Alexander Zhidenko, "Quasinormal modes of black holes: From astrophysics to string theory," Reviews of Modern Physics **83**, 793–836 (2011).
[173] Y. Sekhmani, A. Baruah, A. Al-Badawi, S. K. Maurya, M. K. Jasim, M. Altanji, and S. N. Gashti, "Quasinormal spectra, greybody factors, optical shadows, and light deflection by dyonically charged black holes in metric-affine gravity with torsion and nonmetricity," Chin. J. Phys. **99**, 177–198 (2026).
[174] Tanja Hinderer, Benjamin D. Lackey, Ryan N. Lang, and Jocelyn S. Read, "Tidal deformability of neutron stars with realistic equations of state and their gravitational wave signatures in binary inspiral," Phys. Rev. D **81**, 123016 (2010), arXiv:0911.3535 [astro-ph.HE].
[175] Carlos F. Sopuerta and Nicolas Yunes, "Extreme and Intermediate-Mass Ratio Inspirals in Dynamical Chern-Simons Modified Gravity," Phys. Rev. D **80**, 064006 (2009), arXiv:0904.4501 [gr-qc].